The diverse radiodont fauna from the Marjum Formation of Utah, USA (Cambrian: Drumian)

Stephen Pates Corresp., Equal first author, 1 , **Rudy Lerosey-Aubril** Corresp., Equal first author, 1 , **Allison C Daley** 2 , **Carlo Kier** 3 , **Bonino Enrico** 3 , **Javier Ortega-Hernández** 1

1 Museum of Comparative Zoology and Department of Organismic and Evolutionary Biology, Harvard University, Cambridge, Massachusetts, United States

2 Institut des sciences de la Terre (ISTE), Université de Lausanne, Lausanne, Vaud, Switzerland

3 Back to the Past Museum, Carretera Cancún, Quintana Roo, Mexico

Corresponding Authors: Stephen Pates, Rudy Lerosey-Aubril
Email address: stephenpates@fas.harvard.edu, rudy_lerosey@fas.harvard.edu

Radiodonts have long been known from Cambrian deposits preserving non-biomineralizing organisms. In Utah, the presence of these panarthropods in the Spence and Wheeler (House Range and Drum Mountains) biotas is now well-documented. Conversely, radiodont occurrences in the Marjum Formation have remained scarce. Despite the large amount of work undertaken on its diverse fauna, only one radiodont (*Peytoia*) has been reported from the Marjum Biota. In this contribution we quadruple the known radiodont diversity of the Marjum fauna, with the description of the youngest members of two genera, *Caryosyntrips* and *Pahvantia,* and that of a new taxon *Buccaspinea cooperi* gen. et sp. nov. This new taxon can be identified from its large oral cone bearing robust hooked teeth with one, two, or three cusps, and by the unique endite morphology and organisation of its frontal appendages. Appendages of at least 12 podomeres bear six recurved plate-like endites proximal to up to four spiniform distal endites. *Pahvantia hastata* specimens from the Marjum Formation are particularly large, but otherwise morphologically indistinguishable from the carapace elements of this species found in the Wheeler Formation. One of the two new *Caryosyntrips* specimens can be confidently assigned to *C. camurus.* The other bears the largest spines relative to appendage length recorded for this genus, and possesses endites of variable size and unequal spacing, making its taxonomic assignment uncertain. *Caryosyntrips, Pahvantia,* and *Peytoia* are all known from the underlying Wheeler Formation, whereas isolated appendages from the Spence Shale and the Wheeler Formation, previously assigned to *Hurdia,* are tentatively reidentified as *Buccaspinea.* Notably, none of these four genera occurs in the overlying Weeks Formation, providing supporting evidence of a faunal restructuring around the Drumian-Guzhangian boundary. The description of three additional nektonic taxa from the Marjum Formation further documents the higher relative proportion of free-swimming species in this biota compared

to those of the Wheeler and Weeks Lagerstätten. This could be related to a moderate deepening of the basin and/or changing regional ocean circulation at this time.

1   **The diverse radiodont fauna from the Marjum Formation of Utah, USA (Cambrian:**

2   **Drumian)**

4   Stephen Pates[1*], Rudy Lerosey-Aubril[1*], Allison C. Daley[2], Carlo Kier[3], Enrico Bonino[3] &

5   Javier Ortega-Hernández[1]

7   [1]Museum of Comparative Zoology and Department of Organismic and Evolutionary Biology,

8   Harvard University, Cambridge, Massachusetts, USA.

9   [2] Institut des sciences de la Terre (ISTE), Université de Lausanne, Lausanne, Vaud, Switzerland.

10   [3] Back to the Past Museum, Carretera Cancún, Puerto Morelos, Quintana Roo, Mexico.

11   *These authors equally contributed to this paper

13   Corresponding authors:

14   Stephen Pates, stephenpates@fas.harvard.edu;

15   Rudy Lerosey-Aubril, rudy_lerosey@fas.harvard.edu

18   **Abstract**

19   Radiodonts have long been known from Cambrian deposits preserving non-biomineralizing

20   organisms. In Utah, the presence of these panarthropods in the Spence and Wheeler (House

21   Range and Drum Mountains) biotas is now well-documented. Conversely, radiodont occurrences

22   in the Marjum Formation have remained scarce. Despite the large amount of work undertaken on

23   its diverse fauna, only one radiodont (*Peytoia*) has been reported from the Marjum Biota. In this

24   contribution we quadruple the known radiodont diversity of the Marjum fauna, with the

25   description of the youngest members of two genera, *Caryosyntrips* and *Pahvantia,* and that of a

26   new taxon *Buccaspinea cooperi* gen. et sp. nov. This new taxon can be identified from its large

27   oral cone bearing robust hooked teeth with one, two, or three cusps, and by the unique endite

28   morphology and organisation of its frontal appendages. Appendages of at least 12 podomeres

29   bear six recurved plate-like endites proximal to up to four spiniform distal endites. *Pahvantia*

30   *hastata* specimens from the Marjum Formation are particularly large, but otherwise

31   morphologically indistinguishable from the carapace elements of this species found in the

32   Wheeler Formation. One of the two new *Caryosyntrips* specimens can be confidently assigned to

33   *C. camurus.* The other bears the largest spines relative to appendage length recorded for this

34   genus, and possesses endites of variable size and unequal spacing, making its taxonomic

35   assignment uncertain. *Caryosyntrips, Pahvantia,* and *Peytoia* are all known from the underlying

36   Wheeler Formation, whereas isolated appendages from the Spence Shale and the Wheeler

37   Formation, previously assigned to *Hurdia,* are tentatively reidentified as *Buccaspinea*. Notably,

38   none of these four genera occurs in the overlying Weeks Formation, providing supporting

39   evidence of a faunal restructuring around the Drumian-Guzhangian boundary. The description of

40   three additional nektonic taxa from the Marjum Formation further documents the higher relative

41   proportion of free-swimming species in this biota compared to those of the Wheeler and Weeks

42   Lagerstätten. This could be related to a moderate deepening of the basin and/or changing

43   regional ocean circulation at this time.

45   **Keywords:** Panarthropoda, Hurdiidae, *Buccaspinea, Caryosyntrips, Pahvantia, Peytoia,* Pelagic

46   lifestyle, Miaolingian, Exceptional preservation.

48   **Introduction**

49   Fossil deposits that preserve the remains of both biomineralizing and non-biomineralizing

50   organisms provide key insights into the evolution and ecology of life on Earth not accessible

51   from the shelly fossil record alone. Such exceptional strata, or Konservat-Lagerstätten, have been

52   discovered in Cambrian deposits on all major Cambrian palaeocontinents. Most Konservat-

53   Lagerstätten are known from China and North America (*Muscente et al. 2017*), and although

54   these deposits are not equally prolific in terms of taxonomic diversity and fossil abundance

55   (*Gaines, 2014*), suffer from different taphonomic biases (*Saleh et al. 2020*), and vary at both

56   regional and continental scales (*Holmes et al. 2018; Fu et al. 2019; Nanglu et al. 2020*), they

57   provide congruent pictures of how bilaterian animals diversified, became ecologically

58 significant, and profoundly influenced marine environments at that time (*Budd & Jensen, 2000;*

59 *Butterfield, 2011, 2018; Erwin & Tweedt, 2012; Mángano & Buatois, 2014, 2020; Daley et al.*

60 *2018*). The most abundant and diverse group of these early bilaterians were total-group

61 euarthropods, relatives of modern arachnids, crustaceans, insects, and myriapods. Iconic in

62 Paleozoic exceptionally-preserved faunas, stem-group euarthropods (*sensu Ortega-Hernández,*

63 *2016*) such as 'gilled-lobopodians' and radiodonts have proved critical for our understanding of

64 the early evolution of the phylum (*Budd, 1998; Daley, 2013; Daley et al. 2009, 2018; Cong et al.*

65 *2014; Vannier et al. 2014; Van Roy et al. 2015; Young & Vinther, 2017*).

66   Radiodonts – a diverse extinct group that includes *Anomalocaris* and its relatives – have

67 long been known as comparatively common elements in Cambrian Konservat-Lagerstätten, but

68 an ever-growing body of evidence shows that these organisms occupied a variety of ecological

69 niches and contributed in different ways to the diversity of early animal communities (*Daley &*

70 *Budd, 2010; Daley & Edgecombe 2014; Vinther et al. 2014; Van Roy et al. 2015; Lerosey-Aubril*

71 *& Pates, 2018*; *Liu et al. 2018; Moysiuk & Caron, 2019*). Radiodonts greatly differed in size,

72 ranging from millimetres to meters in length (*Van Roy et al. 2015; Lerosey-Aubril & Pates,*

73 *2018; Liu et al. 2018; Pates et al. 2020*), and had variable body shapes that impacted their

74 swimming capabilities. Radiodonts are typically reconstructed as nektonic animals (also referred

75 to as 'free swimmers' hereafter), with the possible exception of the eudemersal *Cambroraster*

76 (*Moysiuk & Caron 2019; Liu et al. 2020*). Forms with elongate swimming flaps and reduced

77 cephalic sclerites (amplectobeluids and anomalocaridids; *Daley & Edgecombe, 2014; Cong et al.*

78   *2014, 2016, 2017, 2018*; *Liu et al. 2018*) were likely more agile swimmers than those with

79   comparatively reduced, but paired flaps, and cylindrical bodies made semi-rigid by the presence

80   of an elongate cephalic carapace (e.g. the hurdiid *Aegirocassis* and *Hurdia*; *Daley et al. 2009,*

81   *2013; Van Roy et al. 2015*). Swimming power has been shown to increase with the size of

82   swimming flaps (*Usami, 2006*), which are more developed in amplectobeluids and

83   anomalocaridids. These two families of inferred ambush predators also differ from hurdiids by

84   the presence of a large tail fan, a structure that increases manoeuvrability and reduces turning

85   radii, as demonstrated by experimental fluid dynamics (*Sheppard et al. 2018*). Hurdiids may

86   have been adapted for agile swimming at lower speeds, based on the presence of paired body

87   flaps, with the ventral flaps interpreted as being used mainly for propulsion, and the dorsal flaps

88   providing stability and steering particularly during the sustained gliding that likely characterised

89   the swimming motion in suspension feeding taxa (e.g. *Aegirocassis, Pahvantia*) (*Van Roy et al.*

90   *2015; Lerosey & Pates 2018*).

91   This interpretation of radiodonts as ecologically diverse components of early Paleozoic

92   faunas finds additional support in the recent realization that many Cambrian Konservat-

93   Lagerstätten host several representatives of this major group. For instance, radiodonts are

94   represented by at least nine genera in Chengjiang (all localities together; *Zeng et al. 2018*, tab.

95   S1; *Cong et al. 2018; Guo et al. 2019; Liu et al. 2020*), seven genera in the Burgess Shale

96   (*Moysiuk & Caron, 2019; Zeng et al. 2018*, tab. S1) – three to five of them occurring in the most

97   studied localities (*Daley & Budd, 2010; Daley et al. 2013; O'Brien & Caron, 2016*) –, and four

98 genera in the Kinzers Formation (*Pates & Daley, 2019*). Such co-occurrences are made possible

99 by the occupation of different ecological niches, but also reflect patchiness in the preservation of

100 palaeocommunities within these deposits (*Nanglu et al. 2020*). Recent studies in Utah, the home

101 of five Cambrian Konservat-Lagerstätten (*Robison et al. 2015*), have increased the known

102 diversity of the radiodont faunas in the Spence Shale (three genera; *Briggs et al. 2008; Pates &*

103 *Daley, 2017; Pates et al. 2018a*), the Wheeler Formation in the Drum Mountains (three genera;

104 *Halgedahl et al. 2009, fig. 10L; Pates & Daley, 2017; Lerosey-Aubril & Pates, 2018*), and

105 especially the Wheeler Formation in the House Range (at least six genera; *Briggs et al. 2008;*

106 *Pates et al. 2017, 2018a, b; Lerosey-Aubril et al. 2020a*). Only one radiodont genus

107 (*Anomalocaris*) has as-yet been reported from the Weeks Formation (*Lerosey-Aubril et al. 2014*),

108 but this is the least explored and the youngest of the Cambrian Konservat-Lagerstätten of Utah

109 (*Lerosey-Aubril et al. 2018*). By contrast, the Marjum Formation has received considerable

110 attention by both professional and amateur palaeontologists over the last 50 years (e.g. *Robison,*

111 *1991; Bonino & Kier, 2010; Conway-Morris et al. 2015; Robison et al. 2015*), and yet only two

112 specimens of a single radiodont genus, *Peytoia,* have been described until now (*Briggs &*

113 *Robison, 1984; Pates et al. 2018a*). This is all the more surprising as the Marjum fauna is

114 particularly diverse (over 139 species according to *Robison et al. 2015*, but see below) with a

115 high proportion of pelagic taxa (more than one third of the generic diversity; see definition of

116 pelagic below).

117   In this contribution, we report the first occurrences in the Marjum Formation, and the

118   youngest occurrences overall, of the radiodont genera *Caryosyntrips* and *Pahvantia,* alongside

119   the description of the new hurdiid *Buccaspinea cooperi* gen. et sp. nov. Beyond complementing

120   our understanding of these genera, the new data confirm that the Marjum assemblage is

121   proportionally richer in free swimming components than those of the underlying Wheeler and

122   overlying Weeks formations, which might be due to a local increase in bathymetry of the

123   depositional environment, enhanced faunal mixing resulting from changes in ocean circulation,

124   or a combination of these factors.

125

126   **Geological setting**

127   The new radiodont specimens described in this contribution were collected from the Marjum

128   Formation of the House Range of Utah (Fig. 1). This unit was deposited along the northern

129   seaward margin (now western North America) of the 'Great American Carbonate Bank' (*Derby*

130   *et al. 2012*) which encircled Laurentia at this time and separated shallow-water proximal shelf

131   settings from deep-water distal shelf and slope environments. The development of extensive

132   carbonate facies all around Laurentia during the early Cambrian was facilitated by its low-

133   latitude palaeogeographic position (*Torsvik & Cocks, 2017*). The Marjum Formation and other

134   Cambrian Lagerstätten from western North America were deposited close to the equator.

135   The Marjum Formation was deposited within the House Range Embayment, a fault-

136   controlled basin that developed during the Wuliuan age and formed a prominent re-entrant

137   within the offshore margin of the carbonate platform in parts of present-day Nevada and Utah

138   (*Hintze & Robison, 1975*; *Rees, 1986*). This locus of deep-water sedimentation within the Great

139   Carbonate Bank allowed the deposition of a continuous succession of shale-dominated strata

140   typical of the Outer Detrital Belt (*sensu Aitken, 1997*), namely the Wheeler, Marjum, and Weeks

141   Formations (in ascending stratigraphic order). There is clear evidence for the presence of a

142   gently sloping ramp connecting the deepest part of the embayment to the carbonate platform to

143   the east (now north; *Rees, 1986*; *Foster & Gaines, 2016*). In contrast, the transition between the

144   two areas in the west (now south) might have been abrupt (*Rees, 1986*). The Marjum Formation

145   crops out in parts of the House Range of Utah, but not in neighbouring ranges. This more limited

146   geographic extent compared to that of the underlying Wheeler Formation (House Range and

147   Drum Mountains) records a general filling of the basin. Reaching up to ca. 430 m in thickness

148   (*Miller et al. 2012*), the Marjum Formation is composed of thin-bedded limestone inter-bedded

149   with shale/lime mudstone (*Robison, 1964*), which have yielded a diverse biota of about 145

150   species (89 genera), of which 30 are entirely non-biomineralizing organisms (*Robison et al.*

151   *2015*; this study). This important diversity of the Marjum biota is partially explained by the fact

152   that the unit extends from the Drumian to the Guzhangian through three agnostoid biozones

153   (*Ptychagnostus atavus*, *P. punctuosus*, and *Lejopyge laevigata* biozones; *Robison & Babcock,*

154   *2011*). However, to our knowledge non-biomineralized fossils have only been recovered from

155   the middle part of the unit (*P. punctuosus* biozone) and accordingly are all Drumian in age.

156

Material and methods

158 The material described in this contribution consists of new specimens from the Marjum

159 Formation, which are deposited in the collections of the Back to the Past Museum (prefix BPM)

160 and the Natural History Museum of Utah (prefix UMNH.IP). Photographs of additional fossils

161 are used for comparative purposes and to illustrate pelagic components of the Marjum fauna −

162 these specimens are housed in the Biodiversity Institute of the University of Kansas (prefix

163 KUMIP), the Department of Geology of the University of Utah (prefix UU), the Natural History

164 Museum of Utah, and the Smithsonian Institution's U.S. National Museum of Natural History

165 (prefix USNM-PAL). Lastly, materials accessioned at the Museum of Comparative Zoology,

166 Harvard University (prefix MCZ) were examined for comparative purposes but not figured.

167 Details for all specimens considered over the course of this study can be found in the

168 Supplementary Data (*Pates et al. 2020b, Table S1*).

169   *Robison et al.'s* (*2015*) comprehensive list of taxa present in the Wheeler (House Range),

170 Marjum, and Weeks Formations was used to create a database to compare the compositions of

171 their exceptionally-preserved faunas with regard to taxonomy and life habits (*Pates et al. 2020b,*

172 *Supplementary Data 3*). This dataset was refined using taxonomic lists compiled by R. A.

173 Robison, which detail the compositions of fossil assemblages at most Wheeler, Marjum, and

174 Weeks fossil sites in the House Range of Utah. This enabled us to exclude the taxa that only

175 occur in stratigraphic intervals barren of non-biomineralized fossils, such as the lower and upper

176 parts of the Marjum Formation or the lower part of the Weeks Formation. We then updated the

177   resulting dataset to include omitted (*Caron et al. 2013*) or more recently published contributions

178   (*Conway Morris et al. 2015; Maletz & Steiner, 2015; Smith, 2015; Foster & Gaines, 2016;*

179   *Pates et al. 2017; Lerosey-Aubril & Pates, 2018; Lerosey-Aubril & Skabelund, 2018; Lerosey-*

180   *Aubril et al. 2018; Pates et al. 2018a, 2018b; Conway Morris et al. 2020; Lerosey-Aubril et al.*

181   *2020a,b*) and some new discoveries (R.L.-A., pers. obs. 2019). Finally, we complemented the

182   database with information on lifestyle for each taxon. Three broad categories of lifestyles were

183   considered: endobenthic (or infaunal), epibenthic (or epifaunal), and pelagic. Benthic (i.e.

184   bottom-dependent) marine animals are regarded as endobenthic or epibenthic if they spend most

185   of their lives inside the seafloor or on top of it, respectively. An epibenthic lifestyle was also

186   assigned to nektobenthic taxa (*sensu* Whalen & Briggs, 2018) - animals living on the seafloor,

187   but capable of temporary swimming (e.g. most trilobites). We inferred a pelagic lifestyle for

188   animals thought to have spent most of their life within the water column some distance from the

189   seafloor, either as passive drifters (plankton) or active swimmers (nekton).

190   Fossils were photographed dry or immersed in water, under polarized or cross-polarized

191   illumination, using a Nikon D5500 DSLR fitted with a Nikon 40 mm DX Micro-Nikkor lens or a

192   Canon EOS500D digital SLR Camera fitted with a Canon EF-S 60 mm macro lens. In most

193   cases, images were taken with manual focusing through the focal plane and then stacked using

194   Photoshop CC. Images of counterparts were mirrored to orientate features the same way as in the

195   part, thus facilitating direct comparison between figures/figure elements. Image processing

196   software ImageJ and ImageJ2 were used to make digital measurements (*Schneider et al. 2012;*

197   *Rueden et al. 2017*). Interpretative drawings and figures were constructed using Photoshop CC

198   and Inkscape 0.92.

199   The electronic version of this article in Portable Document Format (PDF) will represent a

200   published work according to the International Commission on Zoological Nomenclature (ICZN),

201   and hence the new names contained in the electronic version are effectively published under that

202   Code from the electronic edition alone. This published work and the nomenclatural acts it

203   contains have been registered in ZooBank, the online registration system for the ICZN. The

204   ZooBank LSIDs (Life Science Identifiers) can be resolved and the associated information viewed

205   through any standard web browser by appending the LSID to the prefix http://zoobank.org/. The

206   LSID for this publication is: urn:lsid:zoobank.org:pub:80914DF2-7D3E-4A02-81DE-

207   156F8E70889E. The online version of this work is archived and available from the following

208   digital repositories: PeerJ, PubMed Central and CLOCKSS.

209

210   **Terminology**

211   The terminology used in our descriptions broadly follows *Guo et al. (2019)* and *Lerosey-Aubril*

212   *et al. (2020)* for frontal appendages. The term '*plate-like endite*' is equivalent to 'blade-like

213   endites' (*Guo et al. 2019)*, 'broad, elongate endites' (*Moysiuk & Caron 2019)* and 'elongated

214   ventral spines' *(Daley et al. 2013)* in other recent works. The term '*distal endites*' is used to refer

215   to the simple spiniform endites borne on podomeres distal to those which bear plate-like endites,

216   following *Pates et al. (2019)*. This term is equivalent to 'enditic spines' of *Moysiuk & Caron*

217   *(2019)*. We follow the terminology of *Liu et al. (2020)* for cephalic carapace elements, *Daley &*

218   *Edgecombe (2014)* for trunk parts, and *Daley & Bergström (2012)* for components of the oral

219   cone, with the addition of the term '*tooth'* (used in *Daley et al. 2013* and *Zeng et al. 2018)* to

220   describe spines protruding from the inner margins of oral cone plates. Additional terminology

221   relating to the orientation and measurements of *Caryosyntrips* frontal appendages follows *Pates*

222   *& Daley (2017)*. Abbreviations: sag., sagittal; tr., transverse.

223

224   **Results**

225   **Systematic Palaeontology**

226   Superphylum PANARTHROPODA *Nielsen, 1995*

227   Order RADIODONTA *Collins, 1996*

228   Family HURDIIDAE *Lerosey-Aubril & Pates, 2018*

229

230   *Type genus. Hurdia Walcott, 1912* (including *Proboscicaris Rolfe, 1962*).

231

232   *Other genera included. Aegirocassis Van Roy et al. 2015, Buccaspinea* gen. nov., *Cambroraster*

233   *Moysiuk & Caron, 2019, Cordaticaris Sun et al. 2020, Pahvantia Robison & Richards, 1981,*

234   *Peytoia Walcott, 1911, Stanleycaris Pates et al. 2018b, Ursulinacaris Pates et al. 2019a.*

235   Questionably: *Schinderhannes Kühl et al. 2009, Zhenghecaris Vannier et al. 2006.*

236

237 *Remarks.* The presence of an oral cone made up of plates of different sizes, lightly sclerotized

238 frontal appendages with endites and dorsal spines, and a segmented body covered dorsally by

239 setal structures and bearing triangular lateral flaps allows *Buccaspinea* to be identified as a

240 radiodont. Within Radiodonta, frontal appendages with five or more plate-like endites are only

241 known in members of one family, and so we assign the new taxon to the Hurdiidae.

242   Originally described as a bivalved euarthropod (*Vannier et al. 2006*), *Zhenghecaris*

243 material was later reinterpreted as central carapace elements of a hurdiid radiodont, following

244 comparisons with new putative hurdiid carapace elements from the Chengjiang Biota (*Zeng et al.*

245 *2018*). The main reasoning included comparisons with other material from the same horizons

246 assigned to a new genus, *Tauricornicaris (Zeng et al. 2018).* However, articulated material of

247 *Tauricornicaris latzione,* the type species of this genus*,* demonstrated the presence of articulated

248 tergites in this animal, which indicates a more crownward position in the euarthropod lineage

249 than radiodonts – *Tauricornicaris* is not a hurdiid (*Cong et al. 2018*). This insight in turn led to

250 uncertainty of the reassignment of *Zhenghecaris* to Hurdiidae. Nevertheless, *Zhenghecaris* was

251 included in a recent phylogenetic analysis aimed at understanding the internal relationships of

252 Radiodonta (*Moysiuk & Caron 2019*); there, *Zhenghecaris* was interpreted as central carapace

253 elements with posterolateral spinose processes, and its position was resolved as the sister to

254 *Cambroraster*. The precise systematic position of *Zhenghecaris* remains uncertain pending the

255 discovery of more material that supports radiodont affinities, such as an association with lateral

256 carapace elements or frontal appendages, as similar evidence has recently supported the

257 identification of the previously enigmatic *Pahvantia* as a hurdiid radiodont (*Lerosey-Aubril &*

258 *Pates, 2018)*.

259 The Devonian animal *Schinderhannes* was originally described as a taxon in a crown-

260 ward position relative to Radiodonta, with the support of a phylogenetic analysis (*Kühl et al.*

261 *2009*). More recent studies have supported its identification as a radiodont within a monophyletic

262 Hurdiidae (*Cong et al. 2014; Van Roy et al. 2015; Lerosey-Aubril & Pates, 2018; Moysiuk &*

263 *Caron, 2019*). Its frontal appendages show a comparable organization to hurdiids, but the

264 presence of articulated appendages in the trunk constitutes a major departure from radiodont

265 body plans. Detailed information is still lacking on the structure of the oral cone, presence or

266 absence of dorsal flaps, along with finer details of the frontal appendages, body, and tail, all of

267 which could provide additional support for a radiodont/hurdiid affiliation, or alternative

268 assignment, and so it is left as a questionable member of the family pending future redescription.

269

270 Genus *Buccaspinea* nov.

271 urn:lsid:zoobank.org:act:E69418E9-8933-4ABA-ABBB-17FE5540E5F9

272

273 2013 ? *Hurdia* sp.; *Daley et al.*, p. 35, fig. 24C.

274 2018a ? *Hurdia* sp.; *Pates et al.*, p. 104, tab. 1, figs. 2.3 and 2.4.

275 2020a ? *Hurdia* sp. nov. A; *Lerosey-Aubril et al.*, pp. 7, figs. 3A and 3B.

276

277 *Diagnosis.* Hurdiid radiodont exhibiting the following unique combination of characters: oral

278 cone composed of large and small plates bearing large hooked teeth and surrounding a square

279 central opening ; frontal appendages attach lateral to oral cone and possess at least 12

280 podomeres; six unpaired recurved plate-like endites at least five times longer than the podomeres

281 to which they attach, proximal to considerably shorter (one to two times as long as the height of

282 the podomere to which they attach), spiniform distal endites; auxiliary spines on plate-like

283 endites long and robust, projecting distally; at least 10 trunk segments which do not markedly

284 taper posteriorly; setal structures and broad lateral triangular flaps with transverse lines across

285 their width.

286

287 *Etymology.* From the Latin *'bucca'* (mouth) and *'spinea'* (spiny, thorny), a reference to the

288 distinctive large oral cone bearing large thorn-like teeth for this new taxon.

289

290 *Type material, locality, horizon.* The holotype specimen, BPM 1108 (part and counterpart), an

291 almost complete body lacking carapace elements and compressed in oblique-lateral orientation.

292 This specimen was collected in the Drumian strata (*Ptychagnostus punctuosus* Biozone) of the

293 middle Marjum Formation at the Kells Knolls locality (Fig 1.; locality 1 of *Rigby et al. 2010*;

294 GPS: 39.270709, -113.283868) in the House Range, Millard County, Utah.

295

296   *Additional specimens.* Three isolated frontal appendages flattened in lateral orientation are

297   tentatively assigned to this new taxon. UU18056.34 was recovered from the slightly older

298   Drumian *Ptychagnostus atavus* Biozone of the upper Wheeler Formation at the 'New Dig

299   Quarry' (GPS: 39.35883333, -113.27861111) in the House Range, Millard County, Utah

300   (*Lerosey-Aubril et al. 2020a*). KUMIP 314040 and ROM 59634 originate from the Wuliuan

301   Spence Shale Member (*Ptychagnostus praecurrens* Biozone) of the Langston Formation at the

302   Miners Hollow locality (GPS: 41.6023, -112.0334), Wellsville Mountains, Box Elder County,

303   Utah (*Daley et al. 2013, fig. 24C*; *Pates et al. 2018a, fig 2.3, 2.4*).

304

305   *Buccaspinea cooperi* sp. nov.

306   urn:lsid:zoobank.org:act:80DC43C1-E1A5-4B20-9D7B-D4116122DB85

307   Figures 2–6 [Figure 2 nearby]

308

309   *Diagnosis.* As for genus, by monotypy.

310

311   *Etymology.* The species name *'cooperi'* honours Jason Cooper, who discovered the specimen and

312   made it available for study.

313

314   *Description*. Specimen BPM 1108 (a/b) is a near-complete radiodont body composed of an oral

315   cone, paired frontal appendages, trunk segments, lateral flaps and setal structures, which are

316   preserved in dorsolateral view (Figs. 2, 3). Only the oral cone and frontal appendages are

317   preserved from the head region, and the posterior of the body is not preserved. No eyes, cephalic

318   carapace elements, or internal organs are visible. The specimen measures c. 100 mm (sag.) from

319   the posterior tip of the body to the anterior margin of the oral cone, with the latter structure

320   representing one-quarter of the preserved length (sag.).

321   The oral cone (oc, Figs. 2, 3) is preserved flattened approximately dorsoventrally, and

322   positioned anterior to the trunk. It includes large and small plates (lp, sp, Figs. 4, 5), all bearing

323   prominent multi-pointed teeth along their inner margins. These teeth measure 1–3 mm from base

324   to tip, being largest at the midpoint of each side of the square opening and decreasing in size

325   towards the corners (t, Figs. 4, 5). Each plate bears a tooth with one, two, or three points. For the

326   three-pointed teeth, a large central point is flanked by two smaller points (e.g. white and black

327   arrows in Fig. 6A). Teeth are only visible on two of four internal margins of the central opening.

328   This is due to the slightly oblique orientation of preservation of the oral cone, which has also

329   been compacted as indicated by the overlapping teeth towards the corner of the square opening.

330   The boundaries between the plates in the oral cone are not clear or consistently preserved enough

331   on either part to allow the precise arrangement (e.g. triradial, tetraradial) and number of

332   large/small plates to be determined. However, the clear corner and two straight sides visible in

333   the bottom right region of the central opening are of typical tetraradial arrangement (Fig. 4, 5). In

334   the counterpart, one large plate is visible in the centre of the top row, with smaller plates visible

335   towards both top left and top right corners (lp, sp, Fig. 5). An additional structure is present

336   within the main square opening. This structure, which is fragmented and incomplete, abuts the

337   oral cone along the upper margin of the central opening, and is unlikely to be part of the

338   radiodont mouthparts (om, Figs. 2-5).

339   One frontal appendage is present on each side of the oral cone, with the plate-like

340   endites facing each other (lfa, rfa, Figs. 2, 3). Both frontal appendages are preserved at a slight

341   oblique angle and exhibit podomere boundaries visible as simple lines. The latter allow the

342   recognition of at least 12 podomeres in the left appendage (pd12, Fig. 4); adjacent to the oral

343   cone, a patch of fossil material is tentatively interpreted as the proximal-most part of the shaft

344   region of the appendage (s?, Fig. 4). Only the dorsal margin of the left appendage is visible in the

345   counterpart (lfa, Fig. 5). The total number of podomeres for the right appendage cannot be

346   determined with certainty. At least six large curved, overlapping plate-like endites (en1–6) are

347   delimitated by faint lines on each appendage (en, Figs. 4, 5, 6B; Supplementary Fig. 1). These

348   endites are incomplete in the right appendage, partly due to preparation work that has revealed

349   the outline of the oral cone; when complete, they become progressively shorter towards the distal

350   region of the appendage and their tips are curved (left frontal appendage, Fig. 4). En6 on both

351   appendages bears robust and elongate distally facing auxiliary spines (aux, Figs. 4, 5), the

352   longest of which measure 5.5 mm (right frontal appendage) and 6.5 mm (left frontal appendage)

353   (black arrows, Fig. 4A). On the right appendage, some of those spines belong to more proximal

354   endites and protrude from underneath the distalmost endite (Fig. 6B). Large auxiliary spines can

355   be seen towards the tip of all endites for the left appendage, with the exception of the proximal-

356   most endite. On en6 of the right appendage (Figs. 4, 5, 6B), it can be observed that these spines

357   generally decrease in width and length towards the tip of the endite. Distal to en6 on the same

358   appendage, four much shorter, spiniform endites lacking auxiliary spines can be seen, including a

359   particularly short or incomplete distalmost one (de, Figs. 4, 5; white arrows, Fig. 6B). Due to the

360   curvature of the appendage, these spiniform endites overlie en6, but they can be distinguished

361   from the similarly-sized auxiliary spines attached to this endite by their orientation: the auxiliary

362   spines are perpendicular to the endite to which they attach, whereas these distal endites are not

363   (Fig. 6B). A single of these distal endites is clearly visible on the left appendage (de, Figs. 4, 5).

364   Small triangular dorsal spines are rare but visible on both left and right appendages (ds, Fig. 4)

365   on at least podomeres 5, 9, 10 and 11, suggesting they were likely present along the entire length

366   of the appendage. The base of the terminal spine can be seen on the left appendage (ts, Fig. 4),

367   and the counterpart of the right appendage (ts, Fig. 5). The complete spine is visible only in the

368   right appendage of the part and appears to be long (6.5 mm) and straight, but for a slight kink

369   towards the distal end (ts, Fig. 4). However, it is possible that the morphology of this spine has

370   been obscured by an algal or cyanobacterial filament, because algal or cyanobacterial strands of

371   comparable width can be identified wrapped around dorsal spines of the left appendage (pink

372   strands, Fig. 4), as well as intertwined with some auxiliary spines.

373   The body, which is incomplete at the posterior, curves towards its left from posterior to

374   anterior and does not appear to taper significantly along its preserved length. The number of

375   segments in the trunk cannot be determined from the central region alone, but counting the flaps

376   and the bands of setal structures suggests that it is composed of 11, possibly 12 of them

377   (alternating color bands, Figs. 2 and 3).

378   The anterior three segments appear slightly narrower (tr.) than the rest of the body, as

379   suggested by a comparison of the flap size. The lateral flaps are broad and triangular, and they

380   bear transverse lines running parallel to their long axes over their entire surface (Fig. 6C). Lobe-

381   shaped bands of closely packed, linear-shaped blades parallel to one another and perpendicular to

382   the long axis of the bands, can be seen covering the left set of swimming flaps and the dorsal

383   surface of the body (sb, Figs. 2, 3). The blades change orientation along the length of the band,

384   as shown by the well-preserved organization on the fifth body segment (anteriormost structure

385   labelled 'sb' in Figs. 2, 3). Interpreted as bands of setal blades, these structures overlie the entire

386   width (tr.) of the bases of flaps five to nine on the right side. At the posterior left side of the

387   trunk, a small triangular structure, tentatively interpreted as a lateral flap, is apparently overlain

388   by a band of setal blades (fl? Fig. 3), but the organization of the different elements of the trunk is

389   obscured by their overlap in this area. An alternative interpretation would be that the band of

390   setal blades and putative flap belong to two distinct segments. The posteriormost preserved

391   structure is trapezoidal in outline and has a linear feature along its midline (lin, Figs. 2, 3). The

392   linear feature is most likely the centre of a folded band of setal blades. This indicates that the

393   body was disrupted in some way after deposition on the seafloor, in a process that also removed

394   any evidence of a tail fan, lobes, or spines (if present). Its small size compared to the other setal

395   bands suggests that this may be the beginning of the taper at the posterior of the animal, or could

396   potentially represent the posteriormost set of setal blades.

397

398   *Remarks.* The new taxon displays a number of similarities to other hurdiids, for example in the

399   morphology of its mouthparts and body characters (Table 1). The unique combination of these

400   features, alongside the frontal appendage characters, warrant the erection of a new genus.

401   A tetraradial arrangement of the large plates, as observed in all other hurdiids where the

402   oral cone is well known (*Cambroraster, Cordaticaris, Hurdia, Peytoia;* Table 1) can be

403   tentatively proposed for *Buccaspinea* based on the locations of the large plates – whether these

404   locations are observed or deduced from the positions of the largest marginal teeth – on the sides

405   of the square-like central opening. The best-preserved large plate can be seen on the upper row

406   of plates in the counterpart (lp, Fig. 5) which is approximately at the centre of that row. As the

407   largest teeth are also found at the centre of the lower and right margins of the cone, these would

408   correspond to the position of the large plate on the upper row, and conform to a tetraradial

409   arrangement for this animal. The teeth in the oral cone of the new taxon are longer and broader

410   relative to the central opening and the size of the oral cone than in *Hurdia, Peytoia*, and to a

411   lesser extent *Cordaticaris* (*Daley et al. 2013; Sun et al. 2020), resembling those of

412   *Cambroraster (Moysiuk & Caron, 2019).* The plates of the oral cone in *Cambroraster*, the new

413   taxon, and possibly *Cordaticaris* bear multi-pointed teeth, which reduce in size from the midpoint

414   of the side of the central opening towards the corners (*Moysiuk & Caron 2019,* supplemental

415   figure 6A; *Sun et al. 2020,* fig. 6A, B).

416   The number of flap-bearing trunk segments (not including anterior reduced lamellae or

417   flaps known in *Anomalocaris, Cambroraster, Hurdia* and *Lyrarapax*) described for this new

418   taxon (at least 11) is towards the upper end of what is known in hurdiids (e.g. 11 in *Aegirocassis*

419   and *Peytoia*, eight in *Cambroraster*, six to nine in *Hurdia victoria*), with only *Anomalocaris*

420   *canadensis* (13) reported as having more among radiodonts (*Whittington & Briggs, 1985; Daley*

421   *et al. 2009, 2013; Daley & Edgecombe, 2014; Van Roy et al. 2015; Moysiuk & Caron, 2019).*

422   The anterior three and posteriormost segments appear to be slightly narrower (tr.) compared to

423   most of the body, but otherwise body segments are of a similar size, as inferred from the relative

424   sizes of the flaps and setal structures. This suggests an approximately oblong outline for the

425   body, similar to what is known in *Aegirocassis* and *Hurdia*, and contrasting with the diamond

426   shape and significant posterior taper of *Cambroraster* and *Peytoia*. It is difficult to draw too

427   many similarities in the organisation of the setal structures with other radiodonts, owing to the

428   slight disarticulation of these features in BPM 1108. Setal structures splay over the dorsal surface

429   and the left side and appear to be dorsal to the triangular swimming flaps. It cannot be

430   determined if *Buccaspinea* has the one-dorsal-block arrangement of *Aegirocassis*, *Cordaticaris*

431   and *Peytoia (Whittington & Briggs, 1985; Van Roy et al. 2015; Sun et al. 2020),* or the

432   alternative arrangement of two separate parallel lateral setal bands known in *Hurdia (Daley et al.*

433   *2013*). The lateral triangular flaps exhibit transverse lines across the whole width as in

434   *Aegirocassis, Cambroraster,* and *Hurdia,* although the flaps in *Buccaspinea* are broader than the

435   flaps of these three hurdiids.

436   The organization of the frontal appendages in *Buccaspinea* bears many similarities to

437   what is known for other members of Hurdiidae. Most hurdiid frontal appendages consist of a

438   region formed by five or six podomeres that bear plate-like endites, followed by a distal region in

439   which the podomeres have shorter, often spiniform, endites, or no endites at all. In hurdiids with

440   six plate-like endites (e.g. *Hurdia, Stanleycaris* and a taxon in open nomenclature - ?*Peytoia*

441   from the Tulip Beds), the proximal-most is often morphologically distinct from the remaining

442   ones and has been interpreted as belonging to the shaft region *(Pates et al. 2019a).* The exact

443   morphology of the most proximal of the six endites in this new taxon cannot be determined, but

444   under this hypothesis it would belong to the shaft region, and the remaining five plate-like

445   endites to the distal articulated region. If so, the appendages of this new animal would possess at

446   least 11 podomeres in the distal articulated region, and at least three in the shaft. The recent

447   description of *Cordaticaris,* which exhibits at least eight plate-like endites, suggests that this

448   distinction between shaft and distal articulated region cannot be made on number of endites

449   alone (i.e. hurdiids can have more than five blade-like endites in the distal articulated region),

450   and that a morphological distinction between the shaft endite and endites in the distal articulated

451   region is required to confidently discriminate between these two parts of the appendage. As this

452   cannot be determined for *Buccaspinea,* an alternate interpretation would place all six plate-like

453   endites in the distal articulated region of 12 podomeres, distal to two shaft podomeres lacking

454   endites. Regardless, the endites on the appendages of the new genus reduce slightly in length

455   from proximal to distal, a character that has also been observed in *Hurdia*, and they appear to

456   curve slightly towards the distal portion of the appendage, as seen in *Cambroraster, Hurdia,* and

457   *Stanleycaris.* The elongate nature of the plate-like endites in *Buccaspinea*, which are greater than

458   five times the height of the podomeres to which they attach, is also seen in the filter feeding

459   hurdiids *Aegirocassis* and *Pahvantia,* and to a lesser extent the eudemersal sediment sifter

460   *Cambroraster*, and rare specimens of *Hurdia (Daley et al. 2013; Van Roy et al. 2015; Lerosey-*

461   *Aubril & Pates, 2018; Moysiuk & Caron, 2019)*. The robust and elongate auxiliary spines of

462   *Buccaspinea* bear most similarity to *Cambroraster* and *Hurdia*, and strongly differ from the fine

463   setae of filter feeding hurdiids. It cannot be determined whether these auxiliary spines have

464   hooked tips (see *Moysiuk & Caron, 2019*), but their length relative to endite width is more

465   similar to *Cambroraster* (auxiliary spines of a given endite overlapping two or more endites

466   distally) than *Hurdia.* The (absolute) length of the longest auxiliary spines of *Buccaspinea* is

467   comparable to the maximum length reported from *Hurdia* in the Burgess Shale (6 mm *Daley et*

468   *al. 2013*), and to what is observed in published specimens of *Cambroraster falcatus* (ca. 8 mm,

469   measured digitally from *Moysiuk & Caron, 2019, fig. 2a)*. The presence of shorter spiniform

470   endites lacking auxiliary spines in *Buccaspinea* (de, Figs. 4, 5) is shared with *Cambroraster*

471   *falcatus* (three)*, Hurdia victoria* (one or two)*,* and *Stanleycaris hirpex* (two). *Ursulinacaris*

472   *grallae* also has two distal podomeres bearing reduced spiniform endites, but the latter are paired

473   as are all endites in this taxon (*Pates et al. 2019a*). Most hurdiid frontal appendages terminate in

474 a single or pair of short spines, the terminal spine(s), in which the tips are orientated either

475 dorsally (e.g. *Hurdia*) or ventrally (e.g. *Peytoia nathorsti*). One recently described miniature

476 appendage (ca. 2 mm in length) assigned to Hurdiidae from the Ordovician of Wales displays an

477 elongate straight terminal spine, the length of which is approximately a third of that of the

478 appendage (*Pates et al. 2020*). The terminal spine of this animal also displays a 'U' shaped kink

479 towards its distal end, in the same direction as, but a lower magnitude to, the spine in BPM 1108.

480 These similarities in length (relative to appendage) and shape support the interpretation of the

481 structure protruding from the distal end of the right appendage in *Buccaspinea* as a long terminal

482 spine. In addition, a single specimen of *Caryosyntrips* from the Burgess Shale displays an

483 elongated and apparently flexible projection – albeit thicker than what is observed in

484 *Buccaspinea* and the Welsh hurdiid - at its terminus (*Daley & Budd, 2010, text-fig 6*). On the

485 other hand, algal and cyanobacterial filaments similar in size to this structure are visible around

486 the fossil or associated with prominent parts of it, and therefore a superimposition of a short

487 terminal spine and a single algal or cyanobacterial string cannot be ruled out.

488 One isolated frontal appendage from the Wheeler Formation, House Range (*Lerosey-*

489 *Aubril et al., 2020a, fig. 3A. B*) and two isolated appendage specimens from the Spence Shale

490 (*Daley et al. 2013, fig. 24C, D; Pates et al. 2018a, fig. 2.3, 2.4*) are tentatively assigned to

491 *Buccaspinea*. All three appendages display characteristics of the plate-like endites strongly

492 reminiscent of BPM 1108. The length and curvature of the endites, alongside the relative length

493 and width of auxiliary spines exceed what is generally observed in *Hurdia,* which is the animal

494   with the most similar frontal appendages. However, all three of these specimens from older Utah

495   Lagerstätten apparently exhibit fewer than three spiniform endites in the distal region. If this

496   could be explained by the poor preservation and the orientation of the distal region in two of the

497   specimens from the Spence Shale (*Daley et al. 2013, fig. 24C, D)*, there are not convincing

498   explanations for the fewer number of distal endites observed in the Wheeler specimen and at

499   least one specimen from the Spence Shale (*Pates et al. 2018a, fig 2.3, 2.4)*, hence the only

500   tentative assignment to the new species. All these specimens possess a short terminal spine; if

501   future findings confirm that the terminal spine of *Buccaspinea* frontal appendages is truly

502   elongate, this would preclude these other isolated frontal appendage specimens from being

503   assigned to the new taxon.

504

505   Genus *Pahvantia Robison & Richards, 1981*

506

507   *Type species*. *Pahvantia hastata Robison & Richards, 1981* from the Drumian Wheeler

508   Formation in the House Range of Utah.

509

510   *Diagnosis*. See *Lerosey-Aubril & Pates (2018)*.

511

512   *Pahvantia hastata Robison & Richards, 1981*

513   Figure 7 **[Figure 7nearby]**

514

515   *New material.* UMNH.IP6101, 6105, and 6694, complete or near-complete isolated central

516   cephalic carapace elements; precise origins of these specimens unknown, but associated labels

517   mention the Marjum Formation, which crops out in the House Range of western central Utah,

518   USA; exceptionally-preserved fossils have been recovered from the middle part (30–300 m from

519   base) of this formation only, which belongs to the *Bolaspidella* polymerid trilobite Zone and the

520   *Ptychagnostus punctuosus* agnostoid Zone, Drumian Stage, Miaolingian Series.

521

522   *Description.* The Marjum central carapace elements hardly differ morphologically from

523   previously illustrated *Pahvantia hastata* specimens, despite being more than four times larger

524   than some (lengths >80 mm, sag; UMNH.IP6105 measures 103 mm; *Pates et al. 2020b, Table*

525   *S2*). Yet, they allow the recognition of a few morphological details not previously noticed in the

526   taxon. These larger specimens have a slightly wider (tr.) nuchal region relative to the main

527   region of the element (ca. 10 percent increase of the nuchal region width/main region width

528   ratio), when compared to smaller specimens. In addition, UMNH-IP6101 displays two tiny

529   spines on the posterior margin of its left lateral extension (or 'lappet'; Fig. 7B, D). One of these

530   marginal spines is located where the line marking the boundary between the lateral extension and

531   the main region meets the margin (Fig. 7D). A restudy of previously published material revealed

532   that this inner marginal spine is preserved in at least four other specimens (KUMIP134187 and

533   134879, UMNH.IP6088 and 6093; Fig. 7E–G). In others, no discernible spine occurs, but the

534   margin forms an angle at this point (e.g. KUMIP314089; *Lerosey-Aubril & Pates, 2018*, fig. 1a,

535   b). A second marginal spine is located a short distance abaxially from the first. Its presence could

536   be confirmed in two previously published specimens (KUMIP134187 and 134879; Fig. 7E).

537

538   *Remarks.* This is the first report of the presence of *Pahvantia hastata* in the Marjum Formation,

539   this taxon being hitherto only known from the underlying Wheeler Formation in both the House

540   Range and the Drum Mountains (*Robison & Richards, 1981*; *Lerosey-Aubril & Pates, 2018*;

541   *Lerosey-Aubril et al. 2020a*). The new fossils represent the youngest occurrence of the species

542   and likely extend its biostratigraphical range to the *P. punctuosus* Zone.

543   The larger sizes of these specimens – UMNH.IP6105 is the biggest specimen of the

544   species yet discovered at 103 mm (sag.) – are not necessarily indicative of biological differences

545   between the Wheeler and Marjum assemblages, but may simply stem from a human bias (e.g.

546   preference for larger fossils of the collector). The slight increase of the width of the nuchal

547   region relative to the main region of the central carapace element is the only ontogenetic change

548   detectable in the 17 central carapace elements available for study. Otherwise, the Marjum

549   specimens are strikingly similar to previously described specimens, which confirms that the

550   morphology of this central part of the cephalic carapace was strongly constrained, possibly for

551   functional reasons (*Lerosey-Aubril et al. 2020a*).

552   The marginal spines are reminiscent to those projecting along the posterior margins of

553   the posterolateral extensions in *Cambroraster falcatus* (*Moysiuk & Caron, 2019, figs. 1a, b, g, k,*

554 *sup. figs. 4C, 5D, 7C*). As in *C. falcatus*, marginal spines seem to mark the abaxial limits of the

555 ocular notches, even if the notches in *P. hastata* are represented by concave portions of the

556 margin, rather than actual notches as in *C. falcatus*. Eyes on stalks originating within ocular

557 notches of hurdiid central elements have been described in *Hurdia* (*Daley et al. 2009 fig. 1A, B;*

558 *Daley et al. 2013 fig. 3A, B*), but no marginal spines were identified in this genus, neither in

559 published material, nor in specimens accessioned at the Museum of Comparative Zoology (*Pates*

560 *et al. 2020b, Table S1*). The lateral projections of the central element of putative radiodont

561 *Zhenghecaris shankouensis* also bear spines (one each) along their posterior margins, which

562 might be equivalent to those of the two North American taxa, though substantially more robust

563 (*Zeng et al. 2018, fig. 14A, I*). Lastly, *Sun et al. (2020)* recently described marginal spines in

564 *Cordaticaris* that are similar in number (two per side), location (immediately abaxial to ocular

565 notch), and size (tiny compared to sclerite size) to those of *Pahvantia*, and acknowledged the

566 presence of marginal spines in the latter taxon. These spines represent one of several features of

567 the central carapace element shared by the two taxa (e.g. main region displaying linear pattern,

568 extending into a short anterior spine, and particularly well-differentiated from lateral regions),

569 which suggest a close phylogenetic relationship between them.

570

571 Family uncertain

572 Genus *Caryosyntrips Daley & Budd, 2010*

573

574 *Type species. Caryosyntrips serratus Daley & Budd, 2010,* from the Wuliuan Burgess Shale,

575 British Columbia, Canada.

576

577 *Diagnosis.* See *Pates & Daley (2017).*

578

579 *Caryosyntrips camurus*

580 Figures 8, 9 **[Figure 8 nearby]**

581

582 *Material, locality, horizon.* The material consists of two isolated frontal appendages preserved as

583 lateral compressions. Specimen BPM1100, only tentatively assigned to the species, was collected

584 in the Drumian strata (*Ptychagnostus punctuosus* Biozone) of the middle Marjum Formation at

585 the 'Red Wash' locality (locality 716 of Robison & Babcock, 2011; GPS: 39.318275°, -

586 113.272793°), House Range, Millard County, Utah. Specimen UMNH.IP 6122 (a, b) was found

587 in the Marjum Formation, and therefore in the House Range of western central Utah, USA,

588 although its exact origins are unknown.

589

590 *Description.* BPM1100 (Fig. 8) is an isolated frontal appendage that measures ca. 33 mm along

591 the dorsal margin. This specimen is composed of a bell-shaped proximal region (Fig. 8), a

592 rectangular intermediate region (ca. 10 mm along dorsal margin), and a trapezoidal distal region

593 (ca. 16 mm along dorsal margin). The proximal region is separated from the rectangular

594 intermediate region by an arcuate boundary (hatched line in Fig. 8B), marking the presence of a

595 second layer of cuticle distally. The dorsal and ventral margins are separated by ca. 4 mm in the

596 rectangular region. A change in slope on the dorsal margin marks the boundary between the

597 proximal and intermediate regions. In the intermediate region the appendage tapers distally at an

598 angle of 12-13° between dorsal and ventral margins until it reaches half of its proximal height at

599 its obliquely truncated tip. A dark coloured band runs at mid-height of the intermediate and distal

600 regions, and the dorsal margin of this band continues as a line that curves ventrally in the

601 proximal region. Ventral to this band are numerous lines running dorso-ventrally, many of which

602 look like proximal extensions of the endites. Some of these structures likely represent the second

603 row of endites, which have been displaced slightly owing to the rotation of the appendage,

604 whereas others may represent incomplete endites or poorly preserved podomere boundaries.

605 Straight endites, which curve slightly towards the proximal part of the appendage at their distal

606 tips, are closely spaced and attach separately to the ventral portion of the appendage (en, Fig. 8).

607 These endites are of variable length (1.5 to at least 4 mm) and width (0.4 to at least 1.2 mm). The

608 rotation of the appendage cannot account for this variation, as two endites that form a pair (Fig.

609 8) are of a similar width to one another, despite one being in a deeper plane owing to the rotation

610 of the appendage. These endites are substantially slenderer than the largest and widest endites

611 visible on the appendage.

612   A 2.5 mm wide structure at the proximal margin of the ventral surface could represent

613 the broken base of an especially large endite, but this structure has a different texture to the other

614   endites. This putative endite could have lost the outer layer of cuticle, or it may simply represent

615   some associated organic matter in the matrix slightly overlain by the *Caryosyntrips* appendage.

616   Similar associated organic matter is abundant in this specimen, with a similar sized block

617   overlying and obscuring some of the endites. The appendage appears smooth and essentially

618   featureless dorsal to the dark colored band. Faint lines running proximo-ventrally from indents of

619   the dorsal margin are interpreted as weakly-expressed podomere boundaries, and four

620   protrusions from the dorsal surface can be seen (ds, Fig. 8). These protrusions could represent

621   poorly preserved dorsal spines, but are more likely additional associated organic fragments,

622   unrelated to the *Caryosyntrips* appendage.

623   The second specimen, UMNH.IP 6122 (Fig. 9), is an incomplete isolated frontal

624   appendage, which measures ca. 86 mm along the dorsal margin. The specimen is missing the

625   proximal region and parts of the dorsal region. The rectangular intermediate region is bounded

626   proximally by an S-shaped margin, is ca. 17 mm wide (perpendicular distance between dotted

627   lines delineating intermediate region in Fig. 9B) and 20 mm tall (Fig. 9). The trapezoidal distal

628   region measures 69 mm along the dorsal surface, and tapers at an angle of ca. 12° between its

629   dorsal and ventral margins until reaching 3 mm in height at its blunt termination. Faint

630   boundaries separating at least 12 podomeres can be discerned mostly in the dorsal region.

631   Closely spaced endites curve towards the proximal region of the appendage, and vary slightly in

632   length and width (maximum length and width measured are 2 mm and 0.8 mm respectively; en,

633   Fig. 9). At least four projections form the dorsal margin are visible, which potentially represent

634   dorsal spines (ds?, Fig. 9). As these structures are not consistent in terms of their morphology

635   (the proximal-most one is straight, but more distal projections are curved), and abundant organic

636   matter of a similar shape and preservation permeates the matrix, these structures are best

637   interpreted as unrelated to the appendage. Large patches of cuticular material associated with the

638   proximal region, but distinct from it, potentially represent a poorly preserved second appendage

639   (ap2?, Fig. 9).

640

641   *Remarks.* These two specimens are assigned to the genus *Caryosyntrips* based on the presence of

642   a subtriangular outline (when flattened), triangular endites, and incomplete podomere

643   boundaries. These two *Caryosyntrips,* the first reported from the Marjum Formation (Drumian),

644   also represent the youngest occurrence of this genus. Three *Caryosyntrips* species were

645   previously reported from older Miaolingian deposits in Laurentia: *C. camurus* (Spence Shale and

646   Burgess Shale, Wuliuan; *Pates & Daley, 2017*), *C. durus* (Wheeler Formation, Drum Mountains;

647   Drumian; *Pates & Daley, 2017)*, and *C. serratus* (Burgess Shale and Wheeler Formation, House

648   Range*; Daley & Budd, 2010; Pates & Daley, 2017*). The oldest (and largest) member of the

649   genus (*Caryosyntrips* cf. *C. camurus*) is the only known specimen currently described from

650   outside Laurentia (Gondwana, Valdemiedes Formation, Cambrian Stage 4; *Pates & Daley, 2017*)

651   although the affinities of this specimen have been contested (*Gámez Vintaned & Zhuravlev,*

652   *2018*; *Pates et al. 2018b).*

653   The three distinct *Caryosyntrips* species are currently defined by the spinosity of their

654 dorsal margins, orientation of endites, and subtle differences in the outline of the appendage

655 (*Pates & Daley, 2017*). The type species, *C. serratus*, bears a row of closely spaced small spines

656 along the dorsal margin, has distally orientated endites, and has a slightly curved dorsal margin.

657 This contrasts with *C. camurus*, which lacks dorsal spines completely, possesses endites which

658 project closer to perpendicular to the ventral margin (except in one specimen from the Spence

659 Shale; *Pates & Daley, 2017,* fig. 4C), and terminates in three podomeres of a very reduced

660 height. The third species, *C. durus*, bears small spines all along its dorsal margin in addition to

661 one large spine per podomere, and endites close to perpendicular to the ventral margin; the entire

662 appendage is triangular in outline, no subrectangular region being differentiated proximally

663 (*Pates & Daley, 2017*). Appendages of *Caryosyntrips* also display a notable amount of

664 intraspecific variation in general outline and endite pattern (shape, position, size, and number)

665 depending on the quality of preservation and orientation of the material, which may considerably

666 complicate assignment to a given species.

667   The two specimens described here differ in the size, morphology, and spacing of the

668 endites, and the presence/absence of a medial band. The proximal region of *Caryosyntrips*

669 appendages typically display a convex to bell-shaped outline, as observed in BPM 1100 (*Daley*

670 *& Budd, 2010*, text-fig. 5A; *Pates & Daley, 2017*, figs. 3A, C–F). A concave or sigmoidal

671 proximal margin similar to that of UMNH.IP 6122 has been observed in some *Caryosyntrips*

672 specimens (e.g. *Pates & Daley, 2017,* fig. 3B), where the proximal part of the appendage may

673   have broken off along or close to the boundary between two podomeres. Endites projecting

674   approximately perpendicular to the ventral margin as observed in BPM 1100 are known in some

675   specimens of *C. camurus* and *C. durus,* however the substantial size variation of endites is not

676   known in other members of the genus (ratio of endite to appendage is 1:9 in BPM 1100,

677   compared to 1:12 in *C. camurus*; *Pates & Daley, 2017,* fig. 4B, appendix). The endite

678   morphology of UMNH.IP 6122 is most similar to what is seen in the holotype for *C. camurus*

679   (*Pates & Daley 2017*, fig. 4A). The observation of a medial band running through most of the

680   appendage is another distinctive trait of BPM 1100. A comparable feature occurs in a single

681   previously illustrated specimen of *C. serratus* (*Pates & Daley 2017*, fig. 3F) but is unknown in

682   any *C. camurus*. A distinction between the ventral portion, with well-expressed podomere

683   boundaries, and an apparently unsegmented dorsal portion is also clearly expressed in the

684   holotype of the same species, but this specimen lacks a clear medial band (*Pates & Daley 2017*,

685   fig. 3A).

686   Specimen UMNH.IP 6122 can be confidently assigned to *Caryosyntrips camurus*,

687   assuming that the dorsal projections are taphonomic in origin and do not represent poorly

688   preserved dorsal spines. The shape of the appendage, as well as the size, morphology, and

689   spacing of the endites, all fall within the range of what is known for other members of this

690   species (*Pates & Daley, 2017)*. The morphology of the endites is distinct from the only other

691   member of the species from Utah, a partial specimen from the Spence Shale, which displays

692   straight endites with a rounded distal tip (*Pates & Daley, 2017*).

693   The affinities of specimen BPM 1100 are less clear. Again, assuming that the dorsal

694   projections are taphonomic in origin, the lack of dorsal spines with two rows of simple endites

695   fits with the current diagnosis of *C. camurus*. Whereas the endites of BPM 1100 are larger

696   relative to appendage length than any other member of the species (and genus), this would only

697   require a slight increase in the known morphological variation of spine length within the taxon to

698   accommodate this specimen. However, the unequal spacing of paired endites, and their variation

699   in size, along the ventral margin of the appendage are not observed in any *C. camurus* specimen.

700   These characters (spacing and size variation in endites) may warrant the erection of a new

701   *Caryosyntrips* species in the future, but meanwhile we tentatively assign BPM 1100 to *C.*

702   *camurus*.

703   All known species of *Caryosyntrips* are known from Utah Lagerstätten: *C. camurus* in

704   the Spence Shale and Marjum Formation, *C. durus* in the Wheeler strata of the Drum Mountains,

705   *C. serratus* in the Wheeler strata of the House Range), and a potentially novel *Caryosyntrips*

706   species in the Marjum Formation (*Daley & Budd 2010; Pates & Daley, 2017; Lerosey-Aubril et*

707   *al 2020a;* this study).

708

709   **Discussion**

710   ***Ecological diversity of the Marjum radiodont fauna***

711   The fossils described herein quadruple the known radiodont diversity in the Marjum fauna,

712   adding the taxa *Buccaspinea, Caryosyntrips,* and *Pahvantia* to the previously known *Peytoia*.

713   Interestingly, the four Marjum taxa significantly differ from each other in both body and frontal

714   appendage morphologies, which suggests that if they inhabited the waters of the House Range

715   Embayment at the same time, they were probably not ecological competitors (*Daley & Budd,*

716   *2010*). *Pahvantia hastata* was recently shown to possess frontal appendages with numerous

717   densely packed setae, structures consistent with suspension feeding habits (*Lerosey-Aubril &*

718   *Pates, 2018*). Added to an elongate cephalic carapace, this appendicular morphology suggests

719   that *P. hastata* might have inhabited the uppermost layer of the water column, where it fed on

720   micro- to mesoplankton.

721   *Caryosyntrips* is the least well-known representative of the group – only a partial

722   carapace element is known of its non-appendicular anatomy to date (*Daley & Budd 2010*). The

723   characteristics of the frontal appendages in this genus, such as their subtriangular outline and

724   incomplete podomere articulations, are so unique among radiodonts that this taxon is typically

725   recovered outside a monophyletic Radiodonta in phylogenetic analyses (*Vinther et al. 2014;*

726   *Cong et al. 2014; Van Roy et al. 2015; Liu et al. 2018; Lerosey-Aubril & Pates, 2018; Moysiuk*

727   *& Caron 2019*). *Caryosyntrips* is considered as a free swimmer, similar to other radiodonts and

728   closely related taxa, although its body morphology is unknown and so the extent of its swimming

729   abilities and whether it lived close to the seafloor or high in the water column cannot be

730   determined. It has been speculated that the frontal appendages of *Caryosyntrips* may have

731   worked in a coordinated occlusive motion, with the two appendages moving towards one another

732   to grasp or slice food (*Daley & Budd, 2010; Pates et al. 2017)*. The size of these appendages (2–

733   20 cm in length; *Pates & Daley, 2017*) and their peculiar inferred function among radiodonts

734   (operating as a pair) both suggest that adult individuals of *Caryosyntrips* may have fed on much

735   larger items than the micro- to meso-planktonic organisms ingested by *Pahvantia hastata*.

736   The frontal appendages of *Buccaspinea* bear plate-like endites with extremely robust

737   auxiliary spines, whereas its large oral cone is equipped with particularly robust marginal teeth.

738   The overlap of endites with auxiliary spines would have prevented the capture of prey between

739   endites, and so it is inferred that this animal would have used these endites for sweep feeding, as

740   has been suggested for *Cambroraster* and *Hurdia* which have a comparable frontal appendage

741   organization (*Daley et al. 2013; Moysiuk & Caron, 2019).* The large size of the oral cone and

742   robust spines surrounding a square opening strongly suggest that this was used in combination

743   with the appendages for capture and breakdown of prey items, although the exact manner in

744   which the radiodont oral cone functioned is still poorly understood (e.g. *Whittington & Briggs*

745   *1985; Hagadorn et al., 2010; Daley & Bergström 2012).*

746   The diamond-shaped body of *Peytoia*, with two rows of sub-equal swimming flaps

747   rather long ventral flaps and more reduced dorsal ones (*Whittington & Briggs 1985; Daley et al.*

748   *2013; Van Roy et al. 2015;* Fig. 10C) probably conferred significant swimming power, similar to

749   amplectobeluids and anomalocaridids. The presence of dorsal flaps for steering – and potentially

750   also stability in the water column – in *Peytoia* and other hurdiids (*Van Roy et al. 2015*), rather

751   than a tail fan and/or caudal rami, suggests reduced agility for this animal when compared to

752   *Anomalocaris* and *Amplectobelua,* whereas the different frontal appendage morphologies of

753   these taxa imply distinct prey handling methods (*Daley & Budd, 2010).*

754   In summary, the exact autecology of the Marjum radiodonts remains incompletely

755   understood, but there is some evidence that if these taxa truly lived together at a given time, they

756   occupied distinct ecological niches. The positions in the water column that these organisms

757   occupied, their swimming abilities, their sizes at maturity, their feeding mechanics, and the size

758   and origin of the food items they ingested are all factors potentially explaining how these

759   closely-related taxa might have co-occurred in the same ecosystem. This is similar to the

760   ecological structuring at other Cambrian localities where multiple radiodonts are present, notably

761   at the Burgess Shale where up to seven or more radiodont species have been found at the same

762   site, each interpreted to employ a different feeding strategy, presumably to reduce competition

763   (*Daley & Budd 2010*).

764

765   ***Comparison of the Cambrian radiodont faunas from western Utah***

766   The occurrence of four Konservat-Lagerstätten within the Cambrian deposits of the House Range

767   Embayment provides a rare opportunity to study the distribution of different radiodont taxa in

768   both space and time (over ca. 5 million years). Despite the small sample sizes, which are a result

769   of the rare nature of exceptional preservation and significant collecting effort required to obtain

770   radiodont material from these deposits, a comparison of the radiodont faunas of these

771   assemblages (summarized in Table 2) reveals both geographic and temporal signals. Differences

772 are not considered taphonomic in origin as sedimentological studies have demonstrated a similar

773 palaeoenvironmental setting for the Wheeler, Marjum and Weeks Konservat-Lagerstätten in the

774 House Range (Gaines & Droser, 2005, 2010; Gaines et al. 2005; Lerosey-Aubril et al. 2018). In

775 addition, comparable biostratinomic and geochemical contexts have been reconstructed for the

776 intervals hosting exceptional preservation within the Wheeler and Marjum formations (Gaines &

777 Droser 2010). The only notable taphonomic difference between these deposits is the late

778 diagenetic metamorphism that has affected the Weeks Formation, resulting in a different

779 appearance of the soft-bodied fossils recovered from those beds.

780   The lower Drumian Wheeler biota from the House Range (Wheeler-HR) is most

781 diverse, exemplifying the correlation between taxonomic richness and varied ecological niches

782 within a radiodont assemblage. Taxa with particularly distinctive morphologies are found here

783 (*Lerosey-Aubril et al. 2020a*; *Pates et al. 2017*), in addition to all the forms described in the

784 Marjum Formation. An almost complete body specimen of *Anomalocaris* was reported from this

785 locality by *Briggs et al.* (*2008*), but restudy suggests that it cannot be accommodated within the

786 type-genus of the family Anomalocarididae (work in progress).

787   The coeval Wheeler Formation in the Drum Mountains (Wheeler-DM) differs in both

788 species richness and taxonomic composition (Table 2), sharing only *Pahvantia hastata* with the

789 Wheeler-HR fauna. This may support interpretation of *Pahvantia* as a free swimmer

790 predominantly inhabiting the euphotic zone (*Lerosey-Aubril et al. 2018*), or could simply result

791 from its greater abundance and therefore greater chance of being found, as suggested by the

792   numerous carapace elements recovered in the Wheeler-HR (*Lerosey-Aubril et al. 2020a*). We

793   include an isolated appendage illustrated by *Halgedahl et al.* (*2009*, fig. 10L) in our tally of

794   radiodonts from Wheeler-DM, with its unique combination of features (e.g. tall podomeres, stout

795   spiniform endites alternating in length) likely representing a new anomalocaridid genus. The

796   different compositions of the two Wheeler radiodont assemblages confirm the view that distinct

797   biotas are preserved in the Wheeler strata of the House Range and the Drum Mountains

798   (*Robison, 1991; Robison et al. 2015; Lerosey-Aubril & Skabelund, 2018; Lerosey-Aubril et al.*

799   *2020a*). However, the Wheeler-DM has to date yielded only four radiodont fossils, and

800   additional discoveries could still significantly change the compositions of the Wheeler radiodont

801   faunas.

802   The present contribution significantly increases the known diversity of the Marjum

803   radiodont fauna. Although less species rich, this 'middle' Drumian assemblage is strikingly

804   similar to the slightly older ('lower Drumian') Wheeler-HR radiodont fauna (Table 2).

805   *Pahvantia*, *Peytoia* and possibly *Buccaspinea* are represented by the same species in the

806   Wheeler-HR and the Marjum biotas, whereas distinct species of *Caryosyntrips* occur in these

807   two assemblages and the Wheeler-DM. As to the broader palaeobiogeography of these taxa,

808   *Pahvantia* is endemic to western Utah (*Lerosey-Aubril et al. 2020a*) and *Buccaspinea* to Utah as

809   whole (this study), whereas the Laurentian species of *Peytoia* also occurs in the Wuliuan Spence

810   Shale in northern Utah (e.g. *Pates et al. 2018a*) and the Wuliuan Burgess Shale of British

811   Columbia (e.g. *Daley et al. 2013*). While *Caryosyntrips durus* has a paleobiogeographic range

812   limited to the Wheeler-DM, *C. serratus* and *C. camurus* are known in both Utah (Wheeler-HR,

813   and Marjum and Spence Shale, respectively) and British Columbia (Burgess Shale) (*Pates &*

814   *Daley, 2017*). The complexity of these stratigraphical and palaeogeographical distribution

815   patterns, even locally, suggests notable biological and/or ecological differences between

816   radiodont taxa.

817   Notably, none of the 10 radiodont species recovered from the Wheeler and Marjum

818   Formations has yet been found in the youngest of the Cambrian Lagerstätten of western Utah, the

819   Weeks Formation (Table 2). These Guzhangian strata have yielded two species that are

820   confidently assigned to *Anomalocaris*, even if neither has yet been formally described (*Lerosey-*

821   *Aubril et al. 2014*). Examination of over 800 specimens collected more recently confirms the

822   presence of two taxa, their assignment to *Anomalocaris*, and the small size of the individuals

823   inhabiting the House Range Embayment at that time *(Lerosey-Aubril et al. 2014)*. This genus is

824   otherwise known from older deposits regionally, in the Cambrian Stage 4 Pioche Formation in

825   eastern Nevada (*Lieberman, 2003; Pates et al. 2019b*) and the Spence Shale in northern Utah

826   (*Briggs et al. 2008*). As discussed above, the presence of this genus in the Wheeler-HR is

827   doubtful (*contra Briggs et al. 2008*) and therefore, the Weeks specimens are the only fossils

828   confidently assigned to *Anomalocaris* in the Cambrian of western Utah. The absence of hurdiids

829   in the Weeks assemblage is also particularly striking (Table 2), for they are the most common

830   components of the other Miaolingian radiodont faunas of Utah (including the Spence fauna).

831   Thus, radiodonts confirm the singular composition of the Weeks exceptionally-preserved fauna,

832   a uniqueness that was interpreted as evidence for an important biotic turnover around the

833   Drumian/Guzhangian boundary, at least regionally (*Lerosey-Aubril et al. 2018*).

834

835   ***The Marjum fauna and its pelagic components***

836   The Marjum Formation has yielded 143 species (*Robison et al. 2015*), but this whole unit is

837   particularly thick (ca. 430 m) and spans three agnostoid biozones (*Ptychagnostus atavus*, *P.*

838   *punctuosus*, *Lejopyge laevigata*; *Robison & Babcock, 2011*). Exceptional preservation is

839   confined to the lower part of the *P. punctuosus* Zone only (ca. 30 to 300 m from base; Robison

840   pers. com. 2019), which allows the presently known diversity of this remarkable biota to be

841   quantified at 102 species (82 genera), amongst which 97 (77 genera) represent animals (*Pates et*

842   *al. 2020b, Supplementary Data 3*). Despite this adjustment for stratigraphic position, the Marjum

843   fauna remains the most diverse of the three exceptionally-preserved Miaolingian assemblages of

844   the House Range (HR), those of the Wheeler (*Ptychagnostus atavus* biozone) and Weeks

845   (*Proagnostus bulbus* biozone) Formations totalling 77 and 81 species, respectively. It also differs

846   from these latter two formations by the noticeably greater proportion of pelagic components (Fig.

847   10A–F) – 36% of the generic diversity, against 32% in the Wheeler (HR) and 17% in the Weeks

848   – a pattern reinforced by the new radiodont occurrences reported herein. This richness in pelagic

849   taxa (see definition above) results in part from a greater diversity of agnostoids (Fig. 10A),

850   which comprise no less than 23 species (14 genera). These small euarthropods, considered herein

851   as forming a clade distinct from trilobites (Bergström & Hou 2005; Haug et al. 2010; Edgecombe

852   & Legg 2013), account for 18% of the total generic diversity of the Marjum exceptional fauna,

853   which is twice than what they account for in the Wheeler (HR) and the Weeks faunas. There are

854   slightly more agnostoid genera than trilobite genera in the middle Marjum assemblage, whereas

855   the diversity of trilobites is more than twice that of agnostoids in the other two faunas. The

856   Marjum remarkable fauna is also unique in featuring animals that are extremely rare in Cambrian

857   marine assemblages: jellyfish (*Bonino, 2019)*. Marjum medusiform fossils (Fig. 10B) were

858   described by *Cartwright et al. (2007)*, who interpreted them as the oldest medusoid

859   representatives of three classes of cnidarians (i.e. Cubozoa, Hydrozoa, and Scyphozoa). Other

860   pelagic components include more common taxa, such as radiodonts – previously only known by

861   the sole genus *Peytoia* (Fig. 10C; *Briggs & Robison, 1984*; *Pates et al. 2018a*) – and the

862   'bivalved arthropods' *Branchiocaris*, *Perspicaris*, and *Tuzoia* (Fig. 10D–F; *Robison & Richards,*

863   *1981; Briggs & Robison, 1984*).

864   Interpreting this greater diversity of pelagic components, especially agnostoids, in

865   relation to palaeoenvironmental setting is challenging. Cambrian agnostoids tend to be associated

866   with distal shelf to slope biofacies in low- and mid-latitude regions (e.g. *Robison, 1976;*

867   *Sundberg, 1991; Pegel, 2000; Peng et al., 2012; Hally & Paterson, 2014; Babcock et al. 2015,*

868   *2017*), and many taxa have extensive palaeogeographical ranges allowing their use for

869   intercontinental correlation (*Robison 1976; Peng & Robison, 2000; Peng et al. 2012; Álvaro et*

870   *al. 2013; Babcock et al. 2015, 2017*). Whether agnostoids are interpreted as epibenthic (see

871   definition above) or pelagic organisms (*Esteve & Zamora, 2014* and references therein), the

872   doubling of their specific diversity between the upper Wheeler strata and those of the middle

873   Marjum suggests a deepening of the environment. This observation may appear hard to reconcile

874   with the traditional depiction of a relatively continuous filling of the House Range Embayment

875   through deposition of the Wheeler, Marjum, and Weeks Formations (*Miller et al. 2012*). This

876   general picture is supported by sequence stratigraphy regionally, which shows that the Marjum

877   Formation records variations of sea levels in the forms of third to fifth order cycles, but overall

878   the evolution of the lithofacies up stratigraphy indicates a general shallowing of the depositional

879   environment (*Smith, 2007*). This shallowing trend is materialized by the southward progradation

880   of shallow platform facies down the carbonate ramp forming the northern margin of the basin

881   (*Rees, 1986; Miller et al. 2012*). However, sediment accumulation greatly varied within the

882   basin, which was not filled everywhere at the same rate and the same time. Importantly, *Rees*

883   *(1986)* noted that for most of the existence of the embayment, the low rate of sedimentation in its

884   axial part (e.g. Marjum Pass area) was not sufficient to overcome subsidence, unlike the situation

885   along its northern flank. The inferred relative depth of the central part of the basin somewhat

886   increased during the deposition of the lower (0–200 m) Marjum Formation according to regional

887   sequence stratigraphy (*Smith, 2007*, fig. 30). In other words, while some parts of the basin were

888   being filled, others remained as deep as before or even deepened. Considering that many Marjum

889   localities, including the main sites yielding non-biomineralized fossils (i.e. the Sponge Gully and

890   White Hill localities), correspond to this stratigraphic interval (ca. 30–200 m from base) and

891   geographic area (Marjum Pass and nearby), the observed increase of agnostoid diversity could

892   indeed be interpreted as supporting evidence for a decoupled bathymetric evolution between the

893   axial and marginal parts of the basin. An alternative, or possibly complementary explanation is

894   that the circulation of water in and out of the embayment changed during the Drumian (e.g.

895   stronger landward currents), allowing enhanced faunistic influences of the oceanic province.

896

897   **Conclusions**

898   The discovery of new material from the Marjum Formation continues to highlight the diversity

899   of Utah Konservat-Lagerstätten, and the description of the new taxon *Buccaspinea cooperi*,

900   known only from Utah deposits, further demonstrates the importance of taking a global approach

901   to our understanding of early animal life. The youngest occurrences of two radiodont genera,

902   *Caryosyntrips* and *Pahvantia*, are also reported from the Drumian Marjum Formation in Utah,

903   which brings a total radiodont diversity of this unit to four taxa, the presence of the youngest

904   *Peytoia nathorsti* in these strata being already well established (*Briggs & Robison, 1984; Pates*

905   *et al. 2018a*). These radiodont taxa are all known from the younger Wheeler Formation in the

906   House Range, but contrast with the radiodonts of the younger Weeks Formation (Guzhangian),

907   providing further support for a Guzhangian faunal restructuring, at least regionally. These four

908   radiodonts are interpreted as nektonic, and their discovery further documents the relatively high

909   diversity of pelagic animals in the Marjum Formation, in contrast to the other Lagerstätten of the

910   House Range. This may be the result of a slight deepening of this part of the basin during the

911   Drumian, and/or changing ocean circulation at this time bringing in additional pelagic taxa.

912

Acknowledgements

914   Richard A. Robison generously provided us with critical data on the stratigraphic positions of the

915   Marjum excavation sites and their fossil assemblages they yield. Carolyn Levitt-Bussian and

916   Randal B. Irmis kindly assisted us during our visits to the Natural History Museum of Utah

917   (UMNH) and facilitated the study of the specimens housed in this institution. These specimens

918   were deposited by the Bureau of Land Management, and we particularly thank Scott E. Foss and

919   Greg McDonald, who also provided curatorial assistance. Manuele Bianchi assisted with the loan

920   of BPM 1108 from the Back to the Past Museum to the University of Lausanne. Peter O.

921   Baumgartner (University of Lausanne) permitted the use of their photography equipment at the

922   University of Lausanne. Early drafts of work by paleoartist Holly Sullivan

923   (www.sulscientific.com) helped us to picture how this ecosystem may have looked. Julien

924   Kimmig kindly provided the pictures of KUMIP153917a (*Tuzoia*) and KUMIP2047971a

925   (*Branchiocaris*) illustrated in Figure 10D and F, respectively. Bruce S. Lieberman and Julien

926   Kimmig (KUMIP), and Jessica Cundiff and Mark Renczkowski (MCZ), facilitated study of

927   comparative material. The manuscript benefitted from the fruitful comments of L. Babcock, R.

928   LaVine, and an anonymous referee. We would like to express our sincere gratitude to all of these

929   people for their invaluable help before and during the course of our study.

930

931   **References**

932   Aitken, J.D. 1997. Stratigraphy of the Middle Cambrian platformal succession, southern Rocky

933   Mountains. *Bulletin of the Geological Survey of Canada* **398**, 1–322.

934   Álvaro, J. J., Ahlberg, P., Babcock, L. E., Bordonaro, O. L., Choi, D. K., Cooper, R. A.,

935   Ergaliev, G. K. H., Gapp, I. W., Ghobadi Pour, M., Hughes, N. C., Jago, J. B., Korovnikov, I.,

936   Laurie, J. R., Lieberman, B. S., Paterson, J. R., Pegel, T. V., Popov, L. E., Rushton, A. W. A.,

937   Sukhov, S. S., Tortello, M. F., Zhou, Z. and Żylińska, A. 2013. Global Cambrian trilobite

938   palaeobiogeography assessed using parsimony analysis of endemicity. *Geological Society,*

939   *London, Memoirs* **38**, 273–296.

940   Babcock, L. E., Peng, S. C., Brett, C. E., Zhu, M. Y., Ahlberg, P., Bevis, M. and Robison, R. A.

941   2015. Global climate, sea level cycles, and biotic events in the Cambrian Period. *Palaeoworld*

942   **24**, 5-15.

943   Babcock, L. E., Peng, S. and Ahlberg, P. 2017. Cambrian trilobite biostratigraphy and its role in

944   developing an integrated history of the Earth system. *Lethaia* **50**, 381-399.

945   Doi:10.1111/let.12200.

946   Bergström, J. and Hou, X.-G. 2005. Early Palaeozoic non-lamellipedian arthropods. 73–93. In

947   Koenemann, S. and Jenner, R. A. (eds). Crustacean issues 16: Crustacea and Arthropod

948   Relationships. Taylor and Francis, Boca Raton, FL.

949   Bonino, E. 2019. *Spiagge Cambriane - Meduse e tappeti algali.* Back to the Past Museum,

950   Cancun, 232 pp.

951   Bonino, E. & C. Kier. 2010. *The Back to the Past Museum Guide to Trilobites*. Casa Editrice

952   Marna, Lecco, 494 pp.

953   Briggs, D. E. G. and Robison, R. A. 1984. Exceptionally preserved non-trilobite arthropods and

954   *Anomalocaris* from the Middle Cambrian of Utah. *The University of Kansas*

955   *Paleontological Contributions*, Paper **111**, 1–24.

956   Briggs, D. E. G., Lieberman, B. S., Hendricks, J. R., Halgedahl, S. L. and Jarrard, R. D. 2008.

957   Middle Cambrian arthropods from Utah. *Journal of Paleontology* **82**, 238–254.

958   Budd, G. E. 1998. Stem group arthropods from the Lower Cambrian Sirius Passet fauna of north

959   Greenland. In *Arthropod relationships*, 125–138. Springer, Dordrecht.

960   Budd, G. E. and Jensen, S. 2000. A critical reappraisal of the fossil record of the bilaterian phyla.

961   *Biological Reviews* **75**, 253–295.

962   Butterfield, N. J. 2011. Animals and the invention of the Phanerozoic Earth system. *Trends in*

963   *Ecology and Evolution* **26**, 81–87.

964   Butterfield, N. J. 2018. Oxygen, animals and aquatic bioturbation: an updated account.

965   *Geobiology* **16**, 3–16.

966   Caron, J.-B. and Jackson, D. A. 2008. Paleoecology of the greater phyllopod bed community,

967   Burgess Shale. *Palaeogeography, Palaeoclimatology, Palaeoecology* **258**, 222–256.

968   Caron, J.-B. and Rudkin, D. M. 2009. *A Burgess Shale Primer: History, Geology, and Research*

969   *Highlights. Field Trip Companion Volume, ICCE 2009*. Burgess Shale Consortium,

970   Toronto, 108 pp.

971 Caron, J.-B., Conway Morris, S. and Cameron, C. B. 2013. Tubicolous enteropneusts from the

972   Cambrian period. *Nature* **495**, 503–506.

973 Cartwright, P., Halgedahl, S. L., Hendricks, J. R., Jarrard, R. D., Marques, A. C., Collins, A. G.

974   and Lieberman, B. S. 2007. Exceptionally preserved jellyfishes from the Middle

975   Cambrian. *PLoS ONE* **2(10)**, e1121. doi: 10.1371/journal.pone.0001121

976 Collins, D. 1996. The "evolution" of *Anomalocaris* and its classification in the arthropod Class

977   Dinocarida (nov.) and order Radiodonta (nov.). *Journal of Paleontology* **70**, 280–293.

978 Cong, P., Ma, X., Hou, X., Edgecombe, G. D. and Strausfeld, N. J. 2014. Brain structure resolves

979   the segmental affinity of anomalocaridid appendages. *Nature* **513**, 538–542.

980 Cong, P., Daley, A. C., Edgecombe, G. D., Hou, X. and Chen, A. 2016. Morphology of the

981   radiodontan *Lyrarapax* from the early Cambrian Chengjiang biota. *Journal of*

982   *Paleontology* **90**, 663–671.

983 Cong, P., Daley, A. C., Edgecombe, G. D. and Hou, X. 2017. The functional head of the

984   Cambrian radiodontan (stem-group Euarthropoda) *Amplectobelua symbrachiata*. *BMC*

985   *Evolutionary Biology* **17**, 208.

986 Cong, P. Y., Edgecombe, G. D., Daley, A. C., Guo, J., Pates, S. and Hou, X. G. 2018. New

987   radiodonts with gnathobase-like structures from the Cambrian Chengjiang biota and

988   implications for the systematics of Radiodonta. *Papers in Palaeontology* **4**, 605–621.

989 Conway Morris, S. 1986. The community structure of the middle Cambrian Phyllopod Bed

990   (Burgess Shale). *Palaeontology* **29**, 423–467.

991 Conway Morris, S., Selden, P. A., Gunther, G., Jamison, P. G. and Robison, R. A. 2015. New

992 records of Burgess Shale-type taxa from the middle Cambrian of Utah. *Journal of*

993 *Paleontology* **89**, 411–423.

994 Conway Morris, S., Smith, R. D., Hoyal Cuthill, J., Bonino, E. & Lerosey-Aubril, R. 2020. A

995 possible Cambrian stem-group gnathiferan-chaetognath from the Weeks Formation

996 (Miaolingian) of Utah. *Journal of Paleontology* **94**, 624–636.

997 Daley, A. C. 2013. Anomalocaridids. *Current Biology* **23**, R860–1.

998 Daley, A. C. and Bergström, J. 2012. The oral cone of *Anomalocaris* is not a classic 'Peytoia'.

999 *Naturwissenschaften* **99**, 501–504.

1000 Daley, A. C. and Budd, G. E. 2010. New anomalocaridid appendages from the Burgess Shale,

1001 Canada. *Palaeontology* **53**, 721–38.

1002 Daley, A. C. and Edgecombe, G. D. 2014. Morphology of *Anomalocaris canadensis* from the

1003 Burgess Shale. *Journal of Paleontology* **88**, 68–91.

1004 Daley, A. C., Antcliffe, J. B., Drage, H. B. and Pates, S. 2018. Early fossil record of

1005 Euarthropoda and the Cambrian Explosion. *Proceedings of the National Academy of*

1006 *Sciences* **115**, 5323–5331.

1007 Daley, A. C., Budd, G. E. and Caron, J.-B. 2013. Morphology and systematics of the

1008 anomalocaridid arthropod *Hurdia* from the Middle Cambrian of British Columbia and

1009 Utah. *Journal of Systematic Palaeontology* **11**, 743–87.

1010   Daley, A. C., Budd, G. E., Caron, J.-B., Edgecombe, G. D. and Collins, D. 2009. The Burgess

1011   Shale anomalocaridid *Hurdia* and its significance for early euarthropod evolution. *Science*

1012   **323**, 1597–1600.

1013   Derby, J. R., Fritz, R., Longacre, S. A., Morgan, M. and Sternbach, C. 2012. *The Great*

1014   *American Carbonate Bank: The Geology and Economic Resources of the Cambro-*

1015   *Ordovician Sauk Sequence of Laurentia.* American Association of Petroleum Geologists,

1016   Memoir **98**, 528 pp.

1017   Edgecombe, G. D. And Legg, D. A. 2013. The arthropod fossil record. 393–415. In Minelli, A.,

1018   Boxshall, G. and Fusco, G. (eds). Arthropod biology and evolution. Springer.

1019   Erwin, D. H. and Tweedt, S. 2012. Ecological drivers of the Ediacaran-Cambrian diversification

1020   of Metazoa. *Evolutionary Ecology* **26**, 417–33.

1021   Esteve, J. & Zamora, S. 2014. Enrolled agnostids from Cambrian of Spain provide new insights

1022   about the mode of life in these forms. *Bulletin of Geosciences* **89**, 283–90.

1023   Fletcher, T. P. and Collins, D. H. 1998. The Middle Cambrian Burgess Shale and its relationship

1024   to the Stephen Formation in the southern Canadian Rocky Mountains. *Canadian Journal*

1025   *of Earth Sciences* **35**, 413–436.

1026   Foster, J. R. and Gaines, R. R. 2016. Taphonomy and Paleoecology of the "Middle" Cambrian

1027   (Series 3) Formations in Utah's West Desert: recent finds and new data. 291–336. *In*

1028   Comer, J. B., Inkenbrandt, P. C., Krahulec, K. A. and Pinnell, M. L. (eds). *Resources and*

1029   *Geology of Utah's West Desert*. Utah Geological Association, Publication **45**, 377 pp.

1030   Fu, D., Tong, G., Dai, T., Liu, W., Yang, Y., Zhang, Y., Cui, L., Li, L., Yun, H., Wu, Y., Sun,

1031   A., Cong, L., Pei, W., Gaines, R. R. and Zhang, X. 2019. The Qingjiang biota – a Burgess

1032   Shale–Type fossil Lagerstätte from the early Cambrian of South China. *Science* **363**,

1033   1338–1342.

1034   Gaines, R. R. 2011. New Burgess Shale-type locality in the "thin" Stephen Formation, Kootenay

1035   National Park, British Columbia: stratigraphic and paleoenvironmental setting.

1036   *Paleontographica Canadiana* **31**, 72–88.

1037   Gaines, R. R. 2014. Burgess Shale-type preservation and its distribution in space and time. *The*

1038   *Paleontological Society Papers* **20**, 123–146.

1039   Gaines, R. R. and Droser, M. L. 2005. New approaches to understanding the mechanics of

1040   Burgess Shale-type deposits: from the micron scale to the global picture. *The Sedimentary*

1041   *Record* **3**, 4–8.

1042   Gaines, R. R. and Droser, M. L. 2010. The paleoredox setting of Burgess Shale-type deposits.

1043   *Palaeogeography, Palaeoclimatology, Palaeoecology* **297**, 649–661.

1044   Gaines, R. R., Kennedy, M. J. and Droser, M. L. 2005. A new hypothesis for organic

1045   preservation of Burgess Shale taxa in the Middle Cambrian Wheeler Shale, House Range,

1046   Utah. *Palaeogeography, Palaeoclimatology, Palaeoecology* **220**, 193–205.   Gámez

1047   Vintaned, J. A. G. and Zhuralev, A. Y. 2018. Comment on "*Aysheaia prolata* from the

1048   Utah Wheeler Formation (Drumian, Cambrian) is a frontal appendage of the radiodontan

1049   *Stanleycaris*" by Stephen Pates, Allison C. Daley, and Javier Ortega-Hernández. *Acta*

1050   *Palaeontologica Polonica* **63**, 103–104.

1051   Guo, J., Pates, S., Cong, P., Daley, A. C., Edgecombe, G. D., Chen, T. and Hou, X. 2019. A new

1052   radiodont (stem Euarthropoda) frontal appendage with a mosaic of characters from the

1053   Cambrian (Series 2 Stage 3) Chengjiang biota. *Papers in Palaeontology* **5**, 99–110.

1054   Hagadorn J. W., Schottenfeld M. T. and McGowan D. 2010. Putting *Anomalocaris* on a soft-

1055   food diet? *Geological Society of America Abstracts* **42**, 320.

1056   Halgedahl, S. L., Jarrard, R. D., Brett, C. E. and Allison, P. A. 2009. Geophysical and geological

1057   signatures of relative sea level change in the upper Wheeler Formation, Drum Mountains,

1058   West-Central Utah: a perspective into exceptional preservation of fossils.

1059   *Palaeogeography, Palaeoclimatology, Palaeoecology* **277**, 34–56.

1060   Hally, L. A. and Paterson, J. R. 2014. Biodiversity, biofacies and biogeography of middle

1061   Cambrian (Series 3) arthropods (Trilobita and Agnostida) on the East Gondwana margin.

1062   *Gondwana Research* **26**, 654–674.

1063   Haug, J. T., Maas, A. and Waloszek, D. 2010. *Henningsmoenicaris scutula, Sandtorpia*

1064   *vestrogothienis* gen. et sp. nov. and heterochronic events in early crustacean evolution.

1065   *Transactions of the Royal Society of Edinburgh: Earth Sciences* **100**, 311–350.

1066   Hintze, L. F. 1980. *Geologic map of Utah, scale 1:500,000*. Utah Geological and Mineral

1067   Survey, Salt Lake City.

1068   Hintze, L. F. and Robison, R. A. 1975. Middle Cambrian stratigraphy of the House, Wah Wah,

1069   and adjacent ranges in western Utah. *Bulletin of the Geological Society of America* **86**,

1070   881–891.

1071   Holmes, J. D., García-Bellido, D. C. and Lee, M. S. 2018. Comparisons between Cambrian

1072   Lagerstätten assemblages using multivariate, parsimony and Bayesian methods.

1073   *Gondwana Research* **55**, 30–41.

1074   Hou, X. and Bergström, J. 1997. Arthropods of the Lower Cambrian Chengjiang fauna,

1075   southwewst China. *Fossils & Strata* **45,** 1-116.

1076   Hou, X., Bergström, J. and Ahlberg, P. 1995. *Anomalocaris* and other large animals in the Lower

1077   Cambrian Chengjiang Fauna of southwest China. *GFF* **117**, 163–183.

1078   Kühl, G., Briggs, D. E. and Rust, J. 2009. A great-appendage arthropod with a radial mouth from

1079   the Lower Devonian Hunsrück Slate, Germany. *Science* **323**, 771–773.

1080   Lerosey-Aubril, R. and Pates, S. 2018. New suspension-feeding radiodont suggests evolution of

1081   microplanktivory in Cambrian macronekton. *Nature Communications* **9**, 3774.

1082   doi:10.1038/s41467-018-06229-7

1083   Lerosey-Aubril, R. and Skabelund, J. 2018. *Messorocaris*, a new sanctacaridid-like arthropod

1084   from the middle Cambrian Wheeler Formation (Utah, USA). *Geological Magazine* **155**,

1085   181–186.

1086   Lerosey-Aubril, R., Skabelund, J. and Ortega-Hernández, J. 2020b. Revision of the mollisoniid

1087   chelicerate(?) *Thelxiope*, with a new species from the middle Cambrian Wheeler

1088   Formation of Utah. *PeerJ* **8**, e8879. doi: http://doi.org/10.7717/peerj.8879

1089   Lerosey-Aubril, R., Hegna, T. A., Babcock, L. E., Bonino, E. and Kier, C. 2014. Arthropod

1090   appendages from the Weeks Formation Konservat-Lagerstätte: new occurrences of

1091   anomalocaridids in the Cambrian of Utah, USA. *Bulletin of Geosciences* **89**, 269–282.

1092   Lerosey-Aubril, R., Kimmig, J., Pates, S., Skabelund, J., Weug, A. and Ortega-Hernández, J.

1093   2020a. New exceptionally-preserved panarthropods from the Drumian Wheeler

1094   Konservat-Lagerstätte of the House Range of Utah. *Papers in Palaeontology*. *Online*

1095   *Early View*. doi: https://doi.org/10.1002/spp2.1307

1096   Lerosey-Aubril, R., Gaines, R. R., Hegna, T. A., Ortega-Hernández, J., Van Roy, P., Kier, C. and

1097   Bonino, E. 2018. The Weeks Formation Konservat-Lagerstätte and the evolutionary

1098   transition of Cambrian marine life. *Journal of the Geological Society* **175**, 705–715.

1099   Lieberman, B. S. 2003. A new soft-bodied fauna: the Pioche Formation of Nevada. *Journal of*

1100   *Paleontology* **77**, 674–90.

1101   Liu, J., Lerosey-Aubril, R., Steiner, M., Dunlop, J. A., Shu, D. and Paterson, J.R. 2018. Origin of

1102   raptorial feeding in juvenile euarthropods revealed by a Cambrian radiodontan. *National*

1103   *Science Review* **5,** 863-869.

1104   Liu, Y., Lerosey-Aubril, R., Audo, D., Zhai, D., Mai, H. and Ortega-Hernández J. 2020.

1105   Occurrence of the eudemersal radiodont *Cambroraster* in the early Cambrian Chengjiang

1106   Lagerstätte and the diversity of hurdiid ecomorphotypes. *Geological Magazine* **157**, 1200-

1107   1206. doi: https://doi.org/10.1017/S0016756820000187

1108   Maletz, J. and Steiner, M. 2015. Graptolite (Hemichordata, Pterobranchia) preservation and

1109   identification in the Cambrian Series 3. *Palaeontology* **58**, 1073–1107.

1110   Mángano, M. G. and Buatois, L. A. 2014. Decoupling of body-plan diversification and

1111   ecological structuring during the Ediacaran–Cambrian transition: evolutionary and

1112   geobiological feedbacks. *Proceedings of the Royal Society B: Biological Sciences* **281**,

1113   20140038.

1114   Mángano M.G. and Buatois L.A. 2020. The rise and early evolution of animals: where do we

1115   stand from a trace-fossil perspective? *Interface Focus* **10**, 20190103.

1116   doi.org/10.1098/rsfs.2019.0103

1117   Miller, J. F., Evans, K. R. and Dattilo, B. F. 2012. The Great American Carbonate Bank in the

1118   miogeocline of western central Utah: tectonic influences on sedimentation. 769–854. In

1119   Derby, J. R., Fritz, R., Longacre, S. A., Morgan, M. & Sternbach, C. (eds). *The Great*

1120   *American Carbonate Bank: The Geology and Economic Resources of the Cambro-*

1121   *Ordovician Sauk Sequence of Laurentia*. American Association of Petroleum Geologists,

1122   Memoir, 98, 528 pp.

1123   Moysiuk, J. and Caron, J.-B. 2019. A new hurdiid radiodont from the Burgess Shale evinces the

1124   exploitation of Cambrian infaunal food sources. *Proceedings of the Royal Society B,*

1125   *Biological Sciences* **286**, 20191079. doi: https://dx.doi.org/10.1098/rspb.2019.1079

1126   Muscente, A. D., Schiffbauer, J. D., Broce, J., Laflamme, M., O'Donnell, K., Boag, T. H.,

1127   Meyer, M., Hawkins, A. D., Huntley, J. W., McNamara, M., MacKenzie, L. A., Stanley Jr.,

1128   G. D., Hinman, N. W., Hofmann, M. H. and MacKenzie, L. A. 2017. Exceptionally preserved

1129   fossil assemblages through geologic time and space. *Gondwana Research* **48**, 164–188.

1130   Muscente, A. D., Prabhu, A., Zhong, H., Eleish, A., Meyer, M. B., Fox, P., Hazen, R. M. and

1131   Knoll, A. H. 2018. Quantifying ecological impacts of mass extinctions with network analysis

1132   of fossil communities. *Proceedings of the National Academy of Sciences* **115**, 5217–5222.

1133   Nanglu, K., Caron, J.-B. and Gaines, R. R. 2020. The Burgess Shale paleocommunity with new

1134   insights from Marble Canyon, British Columbia. *Paleobiology* **46**, 58–81.

1135   Nielsen, C. 1995. *Animal evolution: Interrelationships of the living phyla*. Oxford University

1136   Press, Oxford, 402 pp.

1137   O'Brien, L. J. and Caron, J.-B. 2016. Paleocommunity analysis of the Burgess Shale Tulip Beds,

1138   Mount Stephen, British Columbia: comparison with the Walcott Quarry and implications for

1139   community variation in the Burgess Shale. *Paleobiology* **42**, 27–53.

1140   Ortega-Hernández, J. 2016. Making sense of 'lower' and 'upper' stem-group Euarthropoda, with

1141   comments on the strict use of the name Arthropoda von Siebold, 1848. *Biological Reviews* ***91***,

1142   255–273.

1143   Pates, S. and Daley, A. C. 2017. *Caryosyntrips*: a radiodontan from the Cambrian of Spain, USA

1144   and Canada. *Papers in Palaeontology* **3**, 461–470.

1145   Pates, S. and Daley, A. C. 2019. The Kinzers Formation (Pennsylvania, USA): the most diverse

1146   assemblage of Cambrian Stage 4 radiodonts. *Geological Magazine* **156**, 1233–1246.

1147   Pates, S., Daley, A. C. and Butterfield, N. J. 2019a. First report of paired ventral endites in a

1148   hurdiid radiodont. *Zoological Letters* **5**, 18. doi: https://doi.org/10.1186/s40851-019-0132-4

1149   Pates, S., Daley, A. C. and Lieberman, B. S. 2018a. Hurdiid radiodontans from the middle

1150   Cambrian (Series 3) of Utah. *Journal of Paleontology* **92**, 99–113.

1151   Pates, S., Daley, A. C. and Ortega-Hernández, J. 2017. *Aysheaia prolata* from the Utah Wheeler

1152   Formation (Drumian, Cambrian) is a frontal appendage of the radiodontan *Stanleycaris*. *Acta*

1153   *Palaeontologica Polonica* **62**, 619–625.

1154   Pates, S., Daley, A. C. and Ortega-Hernández, J. 2018b. Reply to Comment on "*Aysheaia*

1155   *prolata* from the Utah Wheeler Formation (Drumian, Cambrian) is a frontal appendage of the

1156   radiodontan *Stanleycaris*" with the formal description of *Stanleycaris*. *Acta Palaeontologica*

1157   *Polonica* **63**, 105–110.

1158   Pates, S., Botting, J. P., McCobb, L. M. E. and Muir, L. A. 2020. A miniature Ordovician hurdiid

1159   from Wales demonstrates the adaptability of Radiodonta. *Royal Society Open Science* **7**,

1160   200459. doi: http://dx.doi.org/10.1098/rsos.200459

1161   Pates, S., Daley, A. C., Edgecombe, G. D., Cong, P., and Lieberman, B. S. 2019b. Systematics,

1162   preservation and biogeography of radiodonts from the southern Great Basin, USA, during the

1163   upper Dyeran (Cambrian Series 2, Stage 4). *Papers in Palaeontology*. Online early view.

1164   doi.org/10.1002/spp2.1277

1165   Pates, S., Lerosey-Aubril, R., Daley, A. C., Kier, C., Bonino, E. and Ortega-Hernández, J. 2020b.

1166   Supplementary data for 'The diverse radiodont fauna from the Marjum Formation of Utah,

1167   USA (Cambrian, Drumian)'. *Open Science Framework*. Retrieved from osf.io/y6xwc.

1168   doi.org/10.17605/OSF.IO/Y6XWC

1169   Peng, S. C., Babcock, L. E. and Cooper, R. A. 2012. The Cambrian Period. *In* Gradstein, F. M.,

1170   Ogg, J. G., Schmitz, M. and Ogg, G. J. (eds), *The Geologic Time Scale 2012*, 451–502.

1171   Elsevier, Boston.

1172   Peng, S. C. and Robison, R. A. 2000. Agnostoid biostratigraphy across the Middle-Upper

1173   Cambrian Boundary in China. *Paleontological Society Memoir* **53,** 104. (Supplement to

1174   *Journal of Paleontology* **74**).

1175   Pegel, T. V. 2000. Evolution of trilobite biofacies in Cambrian basins of the Siberian Platform.

1176   *Journal of Paleontology* **74**, 1000–19.

1177   Rees, M. N. 1986. A fault-controlled trough through a carbonate platform: the Middle Cambrian

1178   House Range Embayment. *Geological Society of America Bulletin* **97**, 1054–1069.

1179   Rigby, J. K., Church, S. B. and Anderson, N. K. 2010. Middle Cambrian Sponges from the Drum

1180   Mountains and House Range in Western Utah. *Journal of Paleontology* **84**, 66–78.

1181   Robison, R. A. 1964. Upper Middle Cambrian stratigraphy of western Utah. *Geological Society*

1182   *of America Bulletin* **75**, 995–1010.

1183   Robison, R. A. 1976. Middle Cambrian trilobite biostratigraphy of the Great Basin. *Brigham*

1184   *Young University Geology Studies* **23**, 93-109.

1185   Robison, R. A. 1991. Middle Cambrian biotic diversity: examples from four Utah Lagerstätten.

1186   77–98. *In* Simonetta, A. and Conway Morris, S. (eds). *The Early Evolution of Metazoa*

1187   *and the Significance of Problematic Taxa*. Cambridge University Press, Cambridge, U.K.

1188   Robison, R. A. and Babcock, L. E. 2011. Systematics, paleobiology, and taphonomy of some

1189   exceptionally preserved trilobites from Cambrian Lagerstätten of Utah. *Kansas University*

1190   *Paleontological Contributions* **5**, 1–47.

1191   Robison, R. A. and Richards, B. C. 1981. Larger bivalve arthropods from the Middle Cambrian

1192   of Utah. *The University of Kansas Paleontological Contributions* **106**, 1–28.

1193   Robison, R. A., Babcock, L. E. and Gunther, V. G. 2015. Exceptional Cambrian fossils from

1194   Utah: a window into the age of trilobites. *Utah Geological Survey, Salt Lake City,*

1195   *Miscellaneous Publication* **15-1**, 1–97.

1196   Rolfe, W. D. I. 1962. Two new arthropod carapaces from the Burgess Shale (Middle Cambrian)

1197   of Canada. *Breviora* **160**, 1–9.

1198   Rueden, C. T., Schindelin, J., Hiner, M.C., DeZonia, B. E., Walter, A. E., Arena, E. T. and

1199   Eliceiri, K. W., 2017. ImageJ2: ImageJ for the next generation of scientific image data.

1200   *BMC Bioinformatics* **18**, 529.

1201   Saleh, F., Antcliffe, J.B., Lefebvre, B., Pittet, B., Laibl, L., Peris, F.P., Lustri, L., Gueriau, P. and

1202   Daley, A. C. 2020. Taphonomic bias in exceptionally preserved biotas. *Earth and*

1203   *Planetary Science Letters* **529**, 115873.

1204   Schneider, C. A., Rasband, W. S. and Eliceiri, K. W. 2012. NIH Image to ImageJ: 25 years of

1205   image analysis. *Nature Methods* **9**, 671–675.

1206   Sheppard, K. A., Rival, D. E. and Caron, J.-B. 2018. On the hydrodynamics of *Anomalocaris* tail

1207   fins. *Integrative and Comparative Biology* **58**, 703–711.

1208   Smith, D. D. 2007. *Sequence stratigraphy of the middle Cambrian Marjum Formation: response*

1209   *of sedimentary facies and biota to sea-level changes*. Unpublished MSc. Thesis, Utah State

1210   University, Logan. 156 pp.

1211   Smith, M. R. 2015. A palaeoscolecid worm from the Burgess Shale. *Palaeontology* 58, 973–979.

1212   Sundberg, F. A. 1991. Paleogeography of western Utah and eastern Nevada during the

1213   *Ehmaniella biochron* (Middle Cambrian). *In* Cooper, J. D. and Stevens, C. H. (eds.),

1214   *Paleozoic Paleogeography of the Western United States II*. Pacific Section SEPM **67**, 387–99.

1215   Sun, Z., Zeng, H. and Zhao, F. 2020. A new middle Cambrian radiodont from North China:

1216   Implications for morphological disparity and spatial distribution of hurdiids.

1217   *Palaeogeography, Palaeoclimatology, Palaeoecology*, **558,** 109947.

1218   Torsvik, T. H. and Cocks, L. R. 2017. *Earth History and Palaeogeography*. Cambridge

1219   University Press, Cambridge, 317 pp.

1220   Usami, Y. 2006. Theoretical study on the body form and swimming pattern of *Anomalocaris*

1221   based on hydrodynamic simulation. *Journal of Theoretical Biology* **238**, 11–17.

1222   Vannier, J., Chen, J. Y., Huang, D. Y., Charbonnier, S. and Wang, X. Q. 2006. The early

1223   Cambrian origin of thylacocephalan arthropods. *Acta Palaeontologica Polonica* **51**, 201–

1224   214.

1225   Vannier, J., Liu, J., Lerosey-Aubril, R., Vinther, J. and Daley, A. C. 2014. Sophisticated

1226   digestive systems in early arthropods. *Nature Communications* **5**, 3641.

1227   doi:10.1038/ncomms4641

1228   Van Roy, P., Daley, A. C. and Briggs, D. E. 2015. Anomalocaridid trunk limb homology

1229   revealed by a giant filter-feeder with paired flaps. *Nature* **522**, 77–80.

1230   Vinther, J., Stein, M., Longrich, N. R. and Harper, D. A. 2014. A suspension-feeding

1231   anomalocarid from the Early Cambrian. *Nature* **507**, 496–9.

1232   Whalen, C. D. and Briggs, D. E. (2018). The Palaeozoic colonization of the water column and

1233   the rise of global nekton. *Proceedings of the Royal Society B: Biological Sciences*

1234   **285(1883)**, 20180883.

1235   Walcott, C. D. 1911. Cambrian geology and paleontology II. Middle Cambrian holothurians and

1236   medusa. *Smithsonian Miscellaneous Collections* **57**, 41–68.

1237   Walcott, C. D. 1912. Cambrian geology and paleontology II. Middle Cambrian Branchiopoda,

1238   Malacostraca, Trilobita and Merostomata. *Smithsonian Miscellaneous Collections* **57**,

1239   145–228.

1240   Whittington, H. B. and Briggs, D. E. G.1985. The largest Cambrian animal, *Anomalocaris,*

1241   Burgess Shale, British-Columbia. *Philosophical Transactions of the Royal Society of*

1242   *London, Series B* **309***, 569–609.

1243   Young, F. J. and Vinther, J. 2017. Onychophoran-like myoanatomy of the Cambrian gilled

1244   lobopodian *Pambdelurion whittingtoni. Palaeontology* **60**, 27–54.

1245   Zeng, H., Zhao, F., Yin, Z. and Zhu, M. 2018. Morphology of diverse radiodontan head sclerites

1246   from the early Cambrian Chengjiang Lagerstätte, south-west China. *Journal of Systematic*

1247   *Palaeontology* **16**, 1–37.

1248

1249   **Figure 1. Radiodont occurrences in the Marjum Formation (Cambrian: Drumian) in the**

1250   **House Range of Utah, USA.** (A) Map of western USA showing the locations of the main

1251   Cambrian Konservat-Lagerstätten (circles) of the Great Basin (light grey area), including the

1252   Marjum Formation in the House Range (HR) of western Utah (credit: Rudy Lerosey-Aubril). (B)

1253   Simplified geological map of the central House Range (credit: Rudy Lerosey-Aubril), showing

1254   the geographic distribution of the Marjum Formation and the localities that have yielded

1255   radiodont fossils: Kells Knolls (*Buccaspinea cooperi* gen. et sp. nov.), Red Wash (*Caryosyntrips*

1256   sp.), and Sponge Gully (*Peytoia nathorsti*). A fourth radiodont, *Pahvantia hastata*, occurs in the

1257   Marjum Formation, but the known material of this taxon is of uncertain origin within the House

1258   Range. Data relating to the spatial distributions of Cambrian strata are derived from Hintze

1259   (1980).

1260

1261   **Figure 2. *Buccaspinea cooperi* gen. et sp. nov. from the Marjum Formation (Cambrian:**

1262   **Drumian) in the House Range of Utah, USA.** (A) Part of holotype specimen (BPM 1108a),

1263   general view. (B) Interpretative drawing of (A) (credit: Stephen Pates). Abbreviations: *fl*,

1264   triangular lateral flaps; *lfa*, left frontal appendage; *lin*, linear feature on posteriormost preserved

1265   body segment; *oc*, oral cone; *om*, organic matter inside central opening of the oral cone; *rfa*, right

1266   frontal appendage; *sb*, setal blade.

1267

1268 **Figure 3. *Buccaspinea cooperi* gen. et sp. nov. from the Marjum Formation (Cambrian:**

1269 **Drumian) in the House Range of Utah, USA.** (A) Counterpart of holotype specimen (BPM

1270 1108b), general view (mirrored). (B) Interpretative drawing of (A) (credit: Stephen Pates).

1271 Abbreviations: *fl*, triangular lateral flaps; *lfa*, left frontal appendage; *lin*, linear feature on

1272 posteriormost preserved body segment; *oc*, oral cone; *om*, organic matter; *rfa*, right frontal

1273 appendage; *sb,* setal blade.

1274

1275 **Figure 4. *Buccaspinea cooperi* gen. et sp. nov. from the Marjum Formation (Cambrian:**

1276 **Drumian) in the House Range of Utah, USA.** (A) Part of holotype specimen (BPM 1108a),

1277 detailed view of the oral cone and frontal appendages; black arrows indicate longest auxiliary

1278 spines used for measurements in the main text. (B) Interpretative drawing of (A) (credit: Stephen

1279 Pates). Abbreviations: *aux,* auxiliary spines; *de,* distal endite*; ds,* dorsal spine; *en,* plate-like

1280 endite; *lfa,* left frontal appendage; *lp,* large plate in oral cone; *oc,* oral cone; *om*, organic matter

1281 inside central opening of the oral cone; *pd,* podomere*; rfa,* right frontal appendage; *s,* shaft

1282 podomere; *sb,* setal blade; *sp,* small plate in oral cone*; t,* teeth on inner margin of oral cone*; ts,*

1283 terminal spine.

1284

1285 **Figure 5. *Buccaspinea cooperi* gen. et sp. nov. from the Marjum Formation (Cambrian:**

1286 **Drumian) in the House Range of Utah, USA.** (A) Counterpart of holotype specimen (BPM

1287 1108b), detailed view of the oral cone and frontal appendages; (B) Interpretative drawing of (A)

1288   (credit: Stephen Pates). Abbreviations: *aux*, auxiliary spines; *de,* distal endite*; ds,* dorsal spine;

1289   *en,* plate-like endite; *ir,* inner row of teeth within oral cone; *lfa,* left frontal appendage; *lp*, large

1290   plate; *oc*, oral cone; *om*, organic matter inside central opening of the oral cone; *rfa*, right frontal

1291   appendage; *sb*, setal blade; *t*, teeth on inner margin of oral cone; *ts*, terminal spine.

1292

1293   **Figure 6. *Buccaspinea cooperi* gen. et sp. nov. from the Marjum Formation (Cambrian:**

1294   **Drumian) in the House Range of Utah, USA.** (A, B) Part of holotype specimen (BPM 1108a),

1295   detailed views of the square opening (A) and right frontal appendage (B). (A) details tricuspid

1296   teeth with large central point (black arrow) flanked by two smaller points (white arrows). (B)

1297   shows relationships of terminal spine (pink arrow), auxiliary spines on distalmost plate-like

1298   endite (black arrows), and distal endites (white arrows). (C) Counterpart of holotype specimen

1299   (BPM 1108b), detailed view (mirrored) of posterior flaps showing transverse lines; photographed

1300   under water with cross polarized lighting.

1301

1302   **Figure 7. *Pahvantia hastata* Robison & Richards, 1981, from the Marjum Formation**

1303   **(Cambrian: Drumian) in the House Range of Utah, USA.** All specimens are central carapace

1304   elements photographed using cross-polarization, with their anterior ends towards the top. (A)

1305   Specimen UMNH.IP6694. (B, D) Specimen UMNH.IP6101, general view (B) and detailed view

1306   of the posterior marginal spines (D). (C) Specimen UMNH.IP6105. (E–G) Detailed views of

1307   posterior marginal spines in specimens KUMIP134879 (E), UMNH.IP6088 (F), and

1308 UMNH.IP6093 (G). Abbreviations: *as*, anterior spine; *bo*, boundary between main region and

1309 lateral extension; *cw*, compaction wrinkle; *le*, lateral extension ('lappet'); *li*, lateral indent; *mi*,

1310 median indent; *mr*, main region; *ms*, marginal spine; *nr*, nuchal region; *on*, ocular notch.

1311

1312 **Figure 8. *Caryosyntrips camurus?* from the Marjum Formation (Cambrian: Drumian) in**

1313 **the House Range of Utah, USA.** (A, B) Specimen BPM1100. (A) general view using cross

1314 polarized light. (B) Interpretative drawing (credit: Rudy Lerosey-Aubril). Abbreviations: *ds?*

1315 projection from dorsal surface, potentially a spine; *en*, paired endites; *pm*, bell-shaped posterior

1316 margin.

1317

1318 **Figure 9. *Caryosyntrips camurus* from the Marjum Formation (Cambrian: Drumian) in the**

1319 **House Range of Utah, USA.** (A–C) Specimen UMNH.IP6122. (A, C) general view of (A) part

1320 and (C) counterpart immersed in water (cross polarized light). (B) Composite interpretative

1321 drawing, combining details of both part and counterpart (credit: Rudy Lerosey-Aubril).

1322 Abbreviations: *ap2?*, possible remains of a second appendage; *ds?* projection from dorsal

1323 surface, potentially a spine; *en*, endites; *mo*, mineral outgrowth; *pm*, notched posterior margin.

1324

1325

1326 **Figure 10. Examples of pelagic components of the Marjum Biota (Cambrian: Drumian)**

1327 **from the House Range of Utah, USA.** (A) Agnostoid *Itagnostus interstrictus*, UMNH.IP5621.

1328   (B) Medusiform fossil, UU07021.03 (from *Cartwright et al. 2007*). (C) Radiodont *Peytoia*,

1329   USNM.PAL374593. (D) 'Bivalved arthropod' *Tuzoia*, KUMIP153917a (credit: Julien Kimmig).

1330   (E) 'Bivalved arthropod' *Perspicaris*, UMNH.IP6323. (F) 'Bivalved arthropod' *Branchiocaris*,

1331   KUMIP204797 (credit: Julien Kimmig).

1332

1333   **Supplementary Figure 1. Details of boundaries between endites on appendages of the**

1334   **holotype of *Buccaspinea cooperi* from the Marjum Formation (Cambrian: Drumian) in the**

1335   **House Range of Utah, USA.** (A, C) BPM 1108b, counterpart of holotype. (B, D) BPM 1108a,

1336   part of holotype. Numbers indicate plate-like endites, numbered from proximal to distal. Arrows

1337   indicate boundaries between endites.

Figure 1

Radiodont occurrences in the Cambrian (Drumian) Marjum Formation in the House Range of Utah, USA.

(A) Map of western USA showing the locations of the main Cambrian Konservat-Lagerstätten (circles) of the Great Basin (light grey area), including the Marjum Formation in the House Range (HR) of western Utah (credit: Rudy Lerosey-Aubril). (B) Simplified geological map of the central House Range (credit: Rudy Lerosey-Aubril), showing the geographic distribution of the Marjum Formation and the localities that have yielded radiodont fossils: Kells Knolls (*Buccaspinea cooperi* gen. et sp. nov.), Red Wash (*Caryosyntrips* sp.), and Sponge Gully (*Peytoia nathorsti*). A fourth radiodont, *Pahvantia hastata*, occurs in the Marjum Formation, but the known material of this taxon is of uncertain origin within the House Range. Data relating to the spatial distributions of Cambrian strata are derived from Hintze (1980).

Figure 2

Buccaspinea cooperi gen. et sp. nov. from the Cambrian (Drumian) Marjum Formation in the House Range of Utah, USA.

(A) Part of holotype specimen (BPM 1108a), general view. (B) Interpretative drawing of (A) (credit: Stephen Pates). Abbreviations: *fl*, triangular lateral flaps; *lfa*, left frontal appendage; *lin*, linear feature on posteriormost preserved body segment; *oc*, oral cone; *om*, organic matter inside central opening of the oral cone; *rfa*, right frontal appendage; *sb*, setal blade.
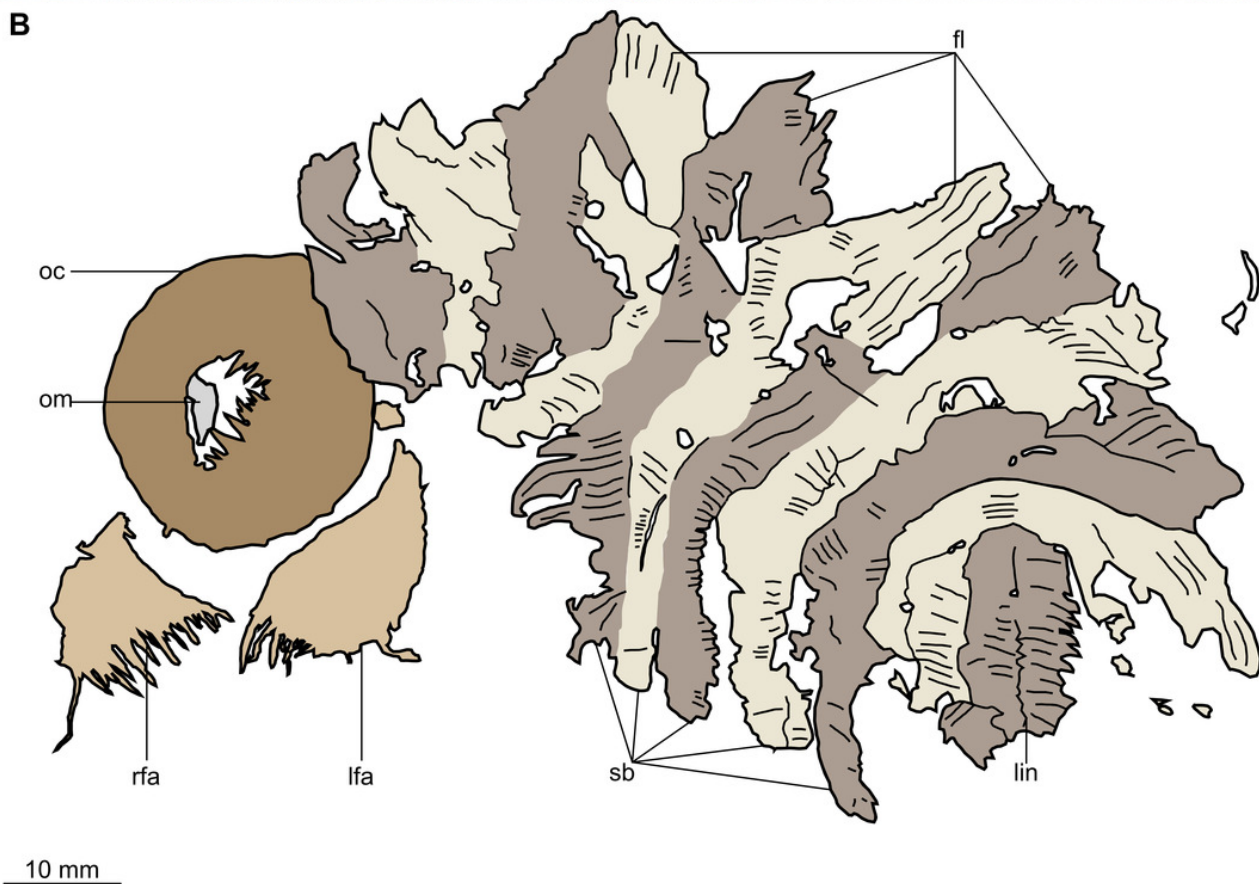
Figure 3

Buccaspinea cooperi gen. et sp. nov. from the Cambrian (Drumian) Marjum Formation in the House Range of Utah, USA.

(A) Counterpart of holotype specimen (BPM 1108b), general view (mirrored). (B) Interpretative drawing of (A) (credit: Stephen Pates). Abbreviations: *fl*, triangular lateral flaps; *lfa*, left frontal appendage; *lin*, linear feature on posteriormost preserved body segment; *oc*, oral cone; *om*, organic matter; *rfa*, right frontal appendage; *sb*, setal blade.
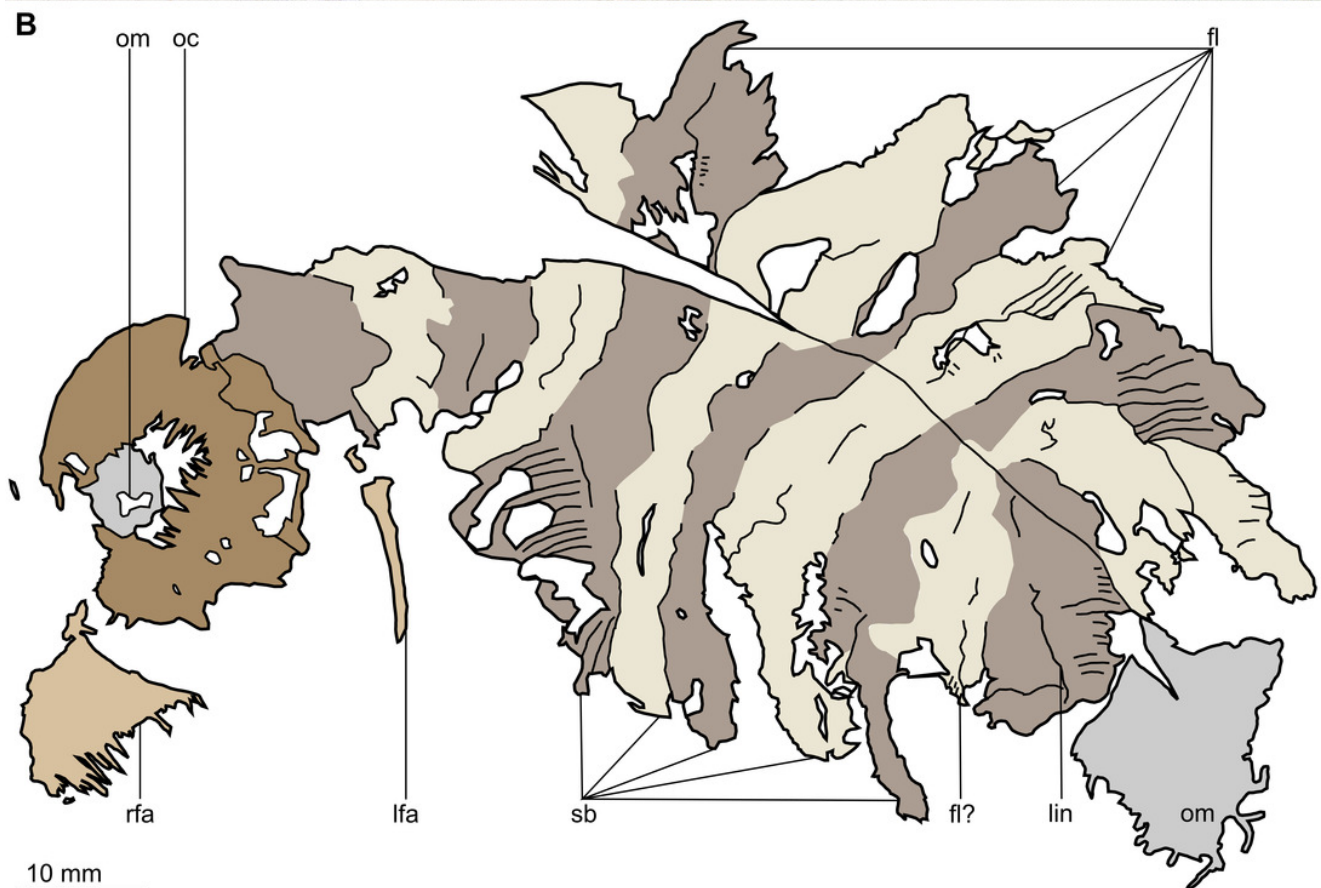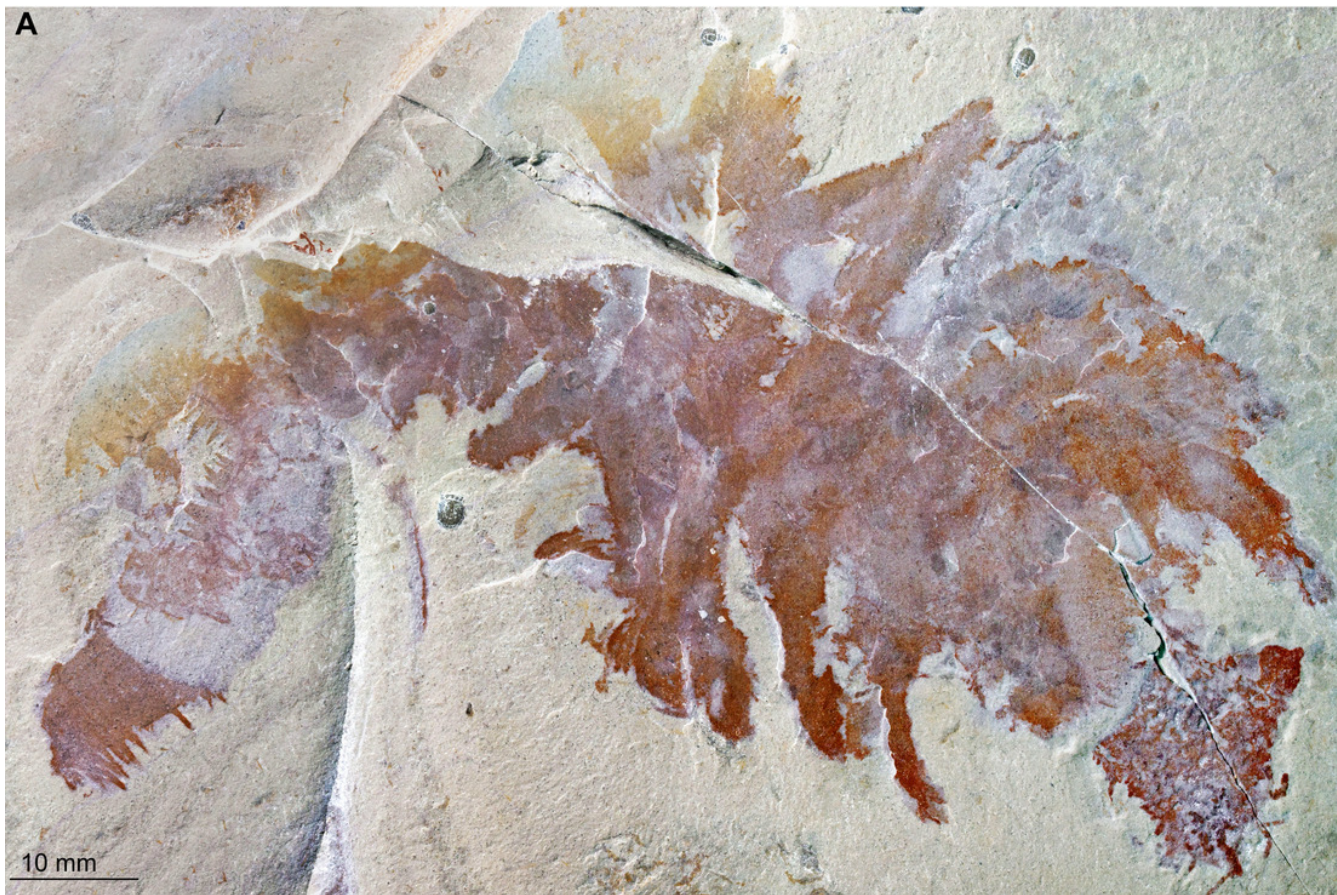
Figure 4

Figure 4. *Buccaspinea cooperi* gen. et sp. nov*.* from the Marjum Formation (Cambrian: Drumian) in the House Range of Utah, USA.

(A) Part of holotype specimen (BPM 1108a), detailed view of the oral cone and frontal appendages; black arrows indicate longest auxiliary spines used for measurements in the main text. (B) Interpretative drawing of (A) (credit: Stephen Pates). Abbreviations: *aux*, auxiliary spines; *de*, distal endite*; ds*, dorsal spine; *en,* plate-like endite; *lfa*, left frontal appendage; *lp*, large plate in oral cone; *oc*, oral cone; *om*, organic matter inside central opening of the oral cone; *pd*, podomere*; rfa*, right frontal appendage; *s*, shaft podomere; *sb*, setal blade; *sp*, small plate in oral cone; *t*, teeth on inner margin of oral cone*; ts*, terminal spine.

Figure 5

Buccaspinea cooperi gen. et sp. nov. from the Cambrian (Drumian) Marjum Formation in the House Range of Utah, USA.

(A) Counterpart of holotype specimen (BPM 1108b), detailed view of the oral cone and frontal appendages; (B) Interpretative drawing of (A) (credit: Stephen Pates). Abbreviations: *aux*, auxiliary spines; *de,* distal endite*; ds*, dorsal spine; *en,* plate-like endite; *ir*, inner row of teeth within oral cone; *lfa*, left frontal appendage; *lp*, large plate; *oc*, oral cone; *om*, organic matter inside central opening of the oral cone; *rfa*, right frontal appendage; *sb*, setal blade; *t*, teeth on inner margin of oral cone; *ts*, terminal spine.
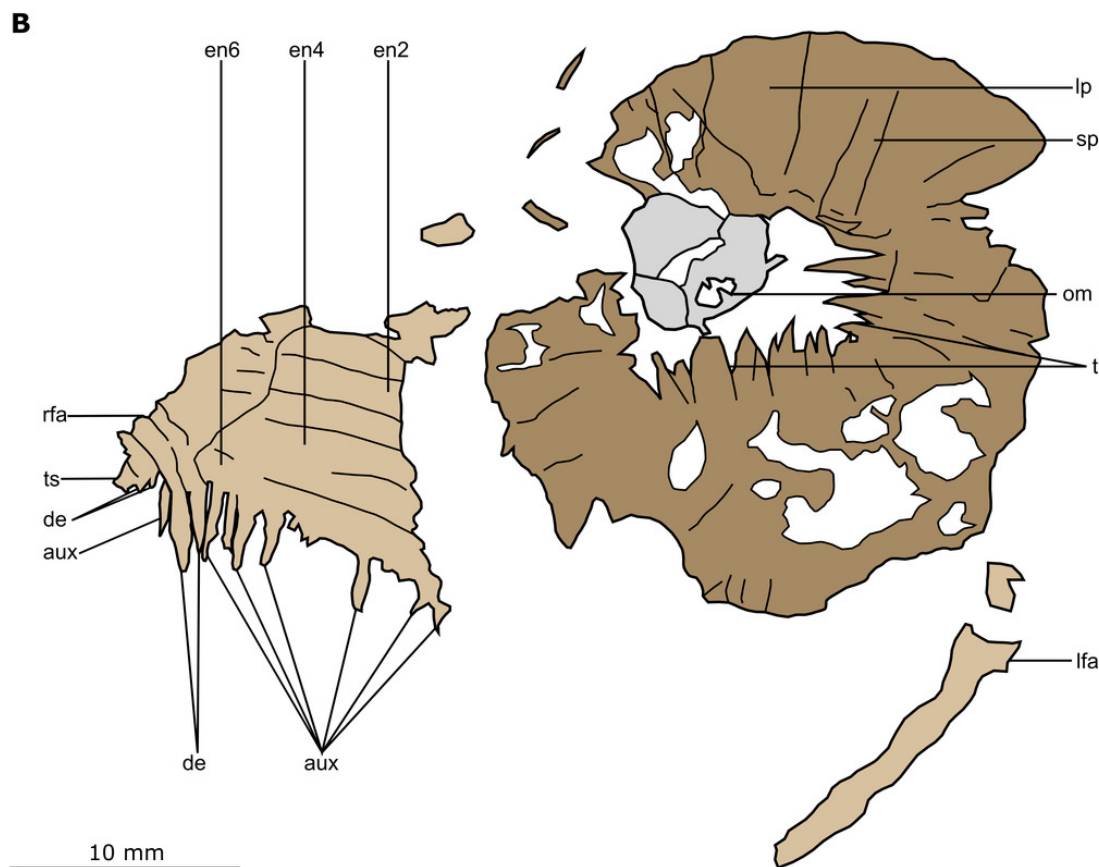
Figure 6

Figure 6. *Buccaspinea cooperi* gen. et sp. nov. from the Marjum Formation (Cambrian: Drumian) in the House Range of Utah, USA.

(A, B) Part of holotype specimen (BPM 1108a), detailed views of the square opening (A) and right frontal appendage (B). (A) details tricuspid teeth with large central point (black arrow) flanked by two smaller points (white arrows). (B) shows relationships of terminal spine (pink arrow), auxiliary spines on distalmost plate-like endite (black arrows), and distal endites (white arrows). (C) Counterpart of holotype specimen (BPM 1108b), detailed view (mirrored) of posterior flaps showing transverse lines; photographed under water with cross polarized lighting.
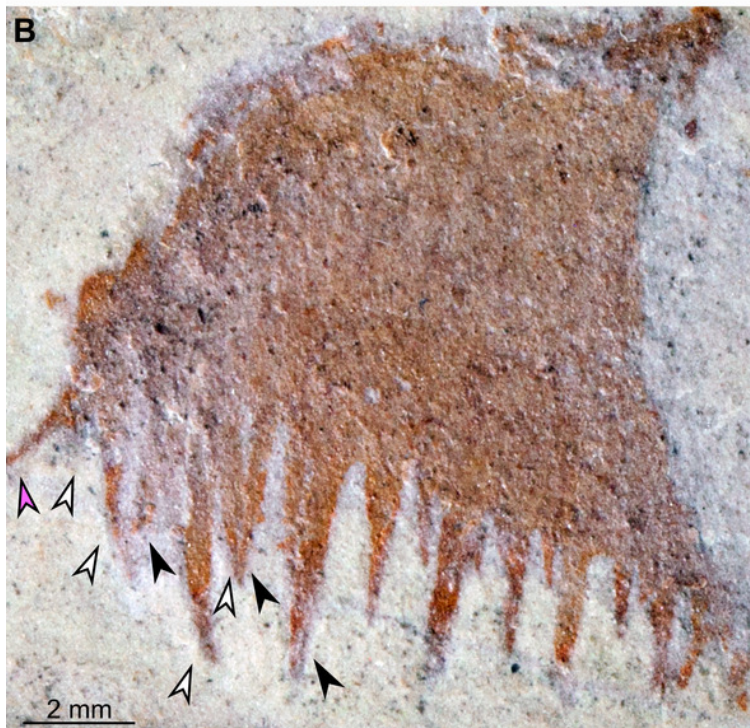
Figure 7

Pahvantia hastata Robison & Richards, 1981, from the Cambrian (Drumian) Marjum Formation in the House Range of Utah, USA.

All specimens are central carapace elements photographed using cross-polarization, with their anterior ends towards the top. (A) Specimen UMNH.IP6694. (B, D) Specimen UMNH.IP6101, general view (B) and detailed view of the posterior marginal spines (D). (C) Specimen UMNH.IP6105. (E–G) Detailed views of posterior marginal spines in specimens KUMIP134879 (E), UMNH.IP6088 (F), and UMNH.IP6093 (G). Abbreviations: *as*, anterior spine; *bo*, boundary between main region and lateral extension; *cw*, compaction wrinkle; *le*, lateral extension ('lappet'); *li*, lateral indent; *mi*, median indent; *mr*, main region; *ms*, marginal spine; *nr*, nuchal region; *on*, ocular notch.
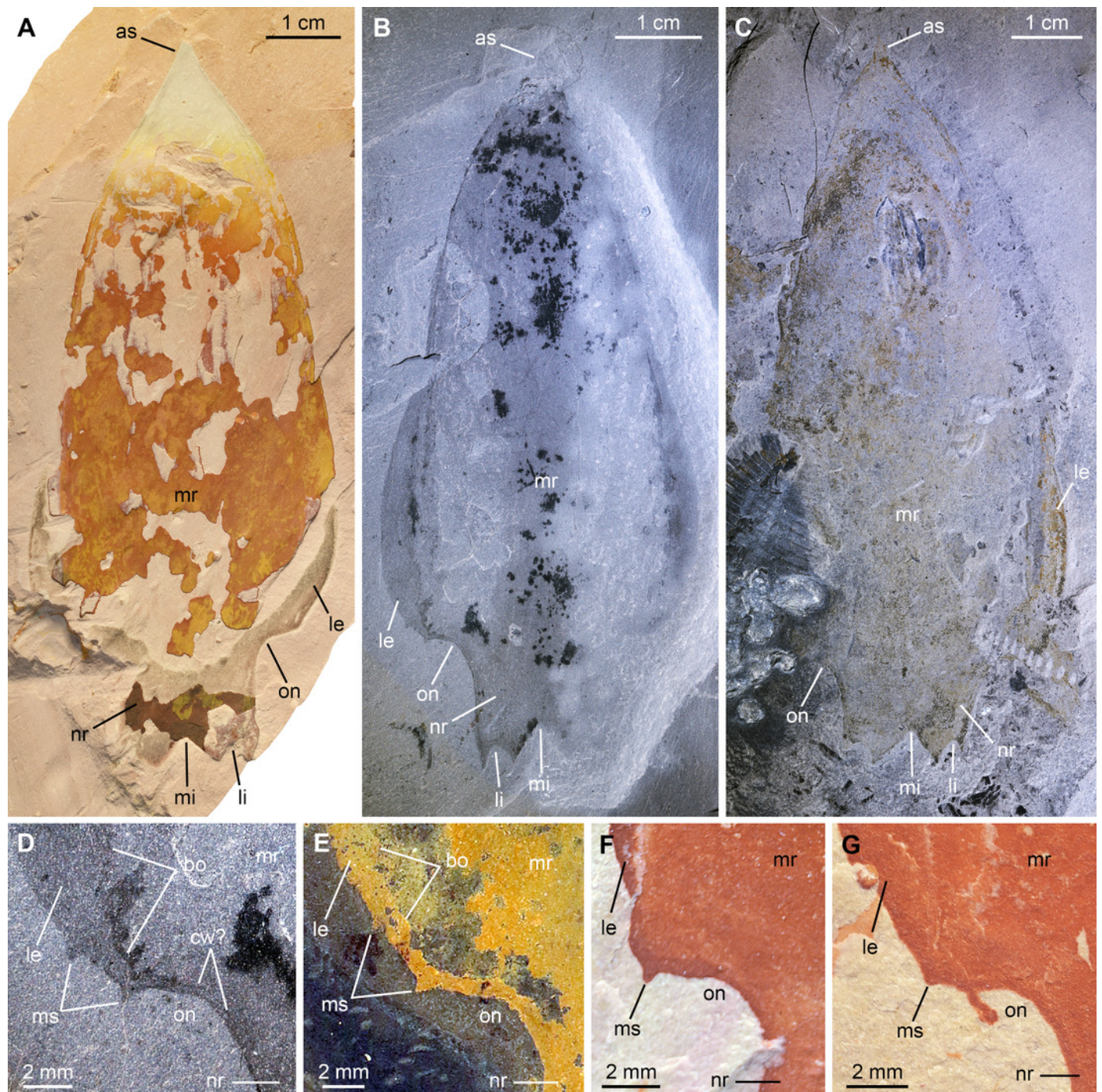
Figure 8

Caryosyntrips camurus? from the Cambrian (Drumian) Marjum Formation in the House Range of Utah, USA.

(A, B) Specimen BPM1100. (A) general view using cross polarized light. (B) Interpretative drawing (credit: Rudy Lerosey-Aubril). Abbreviations: *ds?* projection from dorsal surface, potentially a spine; *en*, paired endites; *pm*, bell-shaped posterior margin.
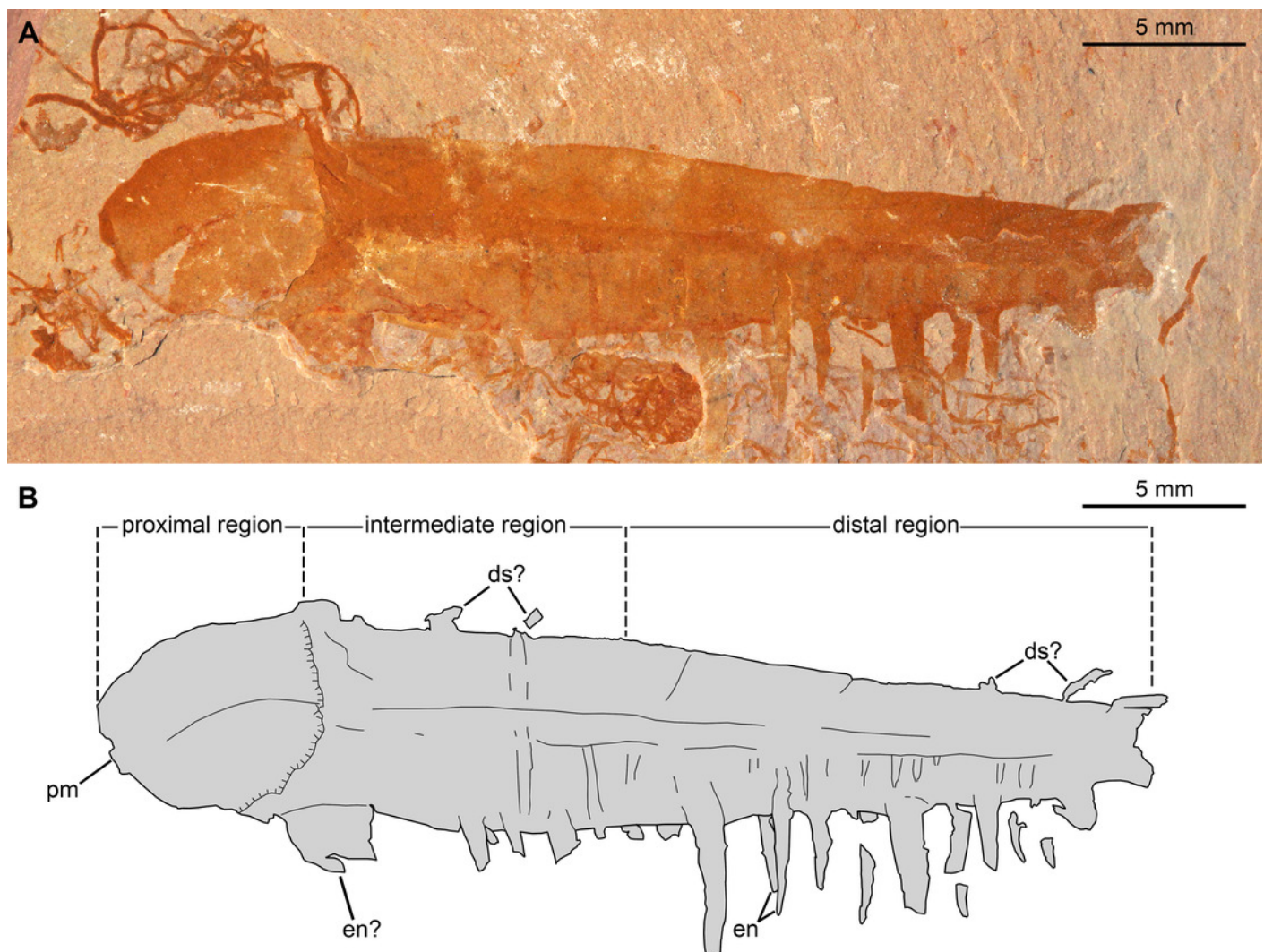
Figure 9

Caryosyntrips camurus from the Cambrian (Drumian) Marjum Formation in the House Range of Utah, USA.

(A–C) Specimen UMNH.IP6122. (A, C) general view of (A) part and (C) counterpart immersed in water (cross polarized light). (B) Composite interpretative drawing, combining details of both part and counterpart (credit: Rudy Lerosey-Aubril). Abbreviations: *ap2?*, possible remains of a second appendage; *ds?* projection from dorsal surface, potentially a spine; *en*, endites; *mo*, mineral outgrowth; *pm*, notched posterior margin.
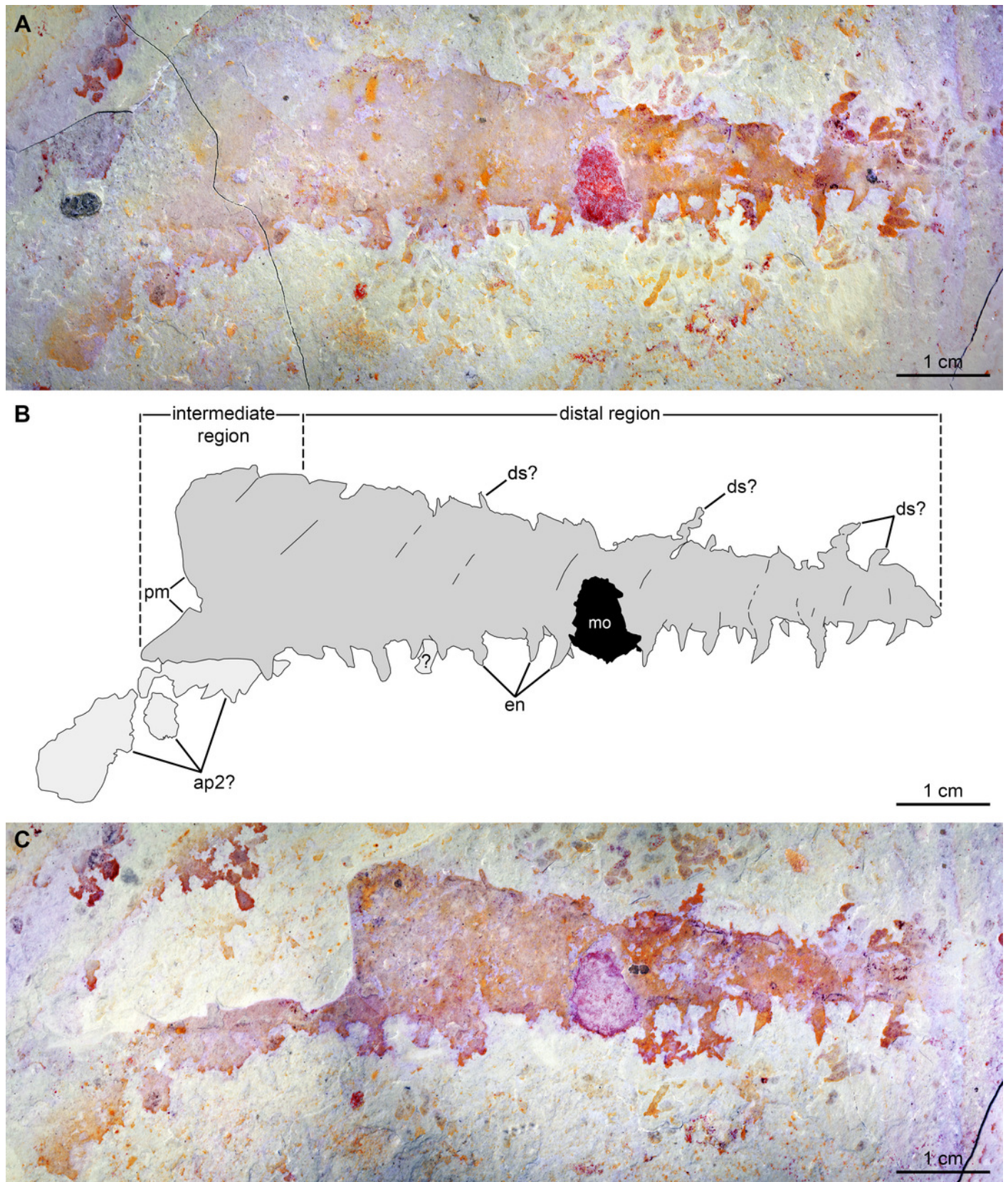
Figure 10

Figure 10. Examples of pelagic components of the Marjum Biota (Cambrian: Drumian) from the House Range of Utah, USA.

(A) Agnostoid *Itagnostus interstrictus*, UMNH.IP5621. (B) Medusiform fossil, UU07021.03 (from *Cartwright et al. 2007*). (C) Radiodont *Peytoia*, USNM.PAL374593. (D) 'Bivalved arthropod' *Tuzoia*, KUMIP153917a (credit: Julien Kimmig). (E) 'Bivalved arthropod' *Perspicaris*, UMNH.IP6323. (F) 'Bivalved arthropod' *Branchiocaris*, KUMIP204797 (credit: Julien Kimmig).
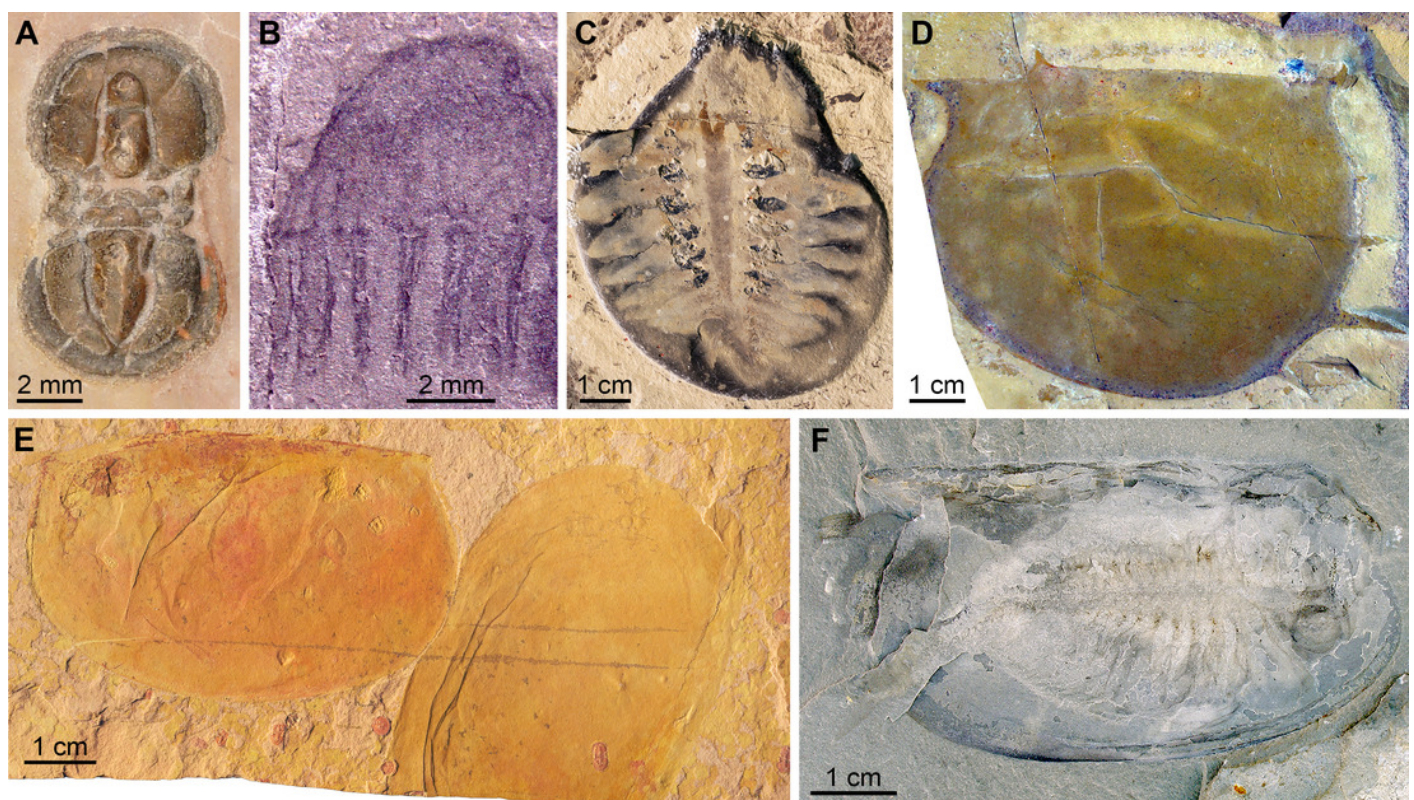
Comparison of the oral cone and trunk morphologies of select hurdiid radiodonts

1   Table 1. Comparison of the oral cone and trunk morphologies of select hurdiid radiodonts.

Anatomical structure	*Aegirocassis*	*Cambroraster*	*Hurdia*	*Peytoia*	*Buccaspinea*
Oral cone					
Symmetry	Unknown	Tetraradial	Tetraradial	Tetraradial	**Tetraradial?**
Marginal teeth	Unknown	Large, three per plate	Small	Small	**Large, hooked, three per plate**
Inner teeth	Unknown	Present	Present	Absent	**Absent**
Body shape	Oblong (weak to no posterior tapering)	Diamond (strong posterior tapering)	Oblong (weak to no posterior tapering)	Diamond (strong posterior tapering)	**Oblong (weak to no posterior tapering)**
Trunk flaps					
Flap-bearing segments[1]	11	8	6–9	11	**11+**
Lateral flap morphology	Small, triangular With transverse lines across entire width	Small, triangular With transverse lines across entire width	Small, triangular With transverse lines across entire width	Broad, triangular With transverse lines across anterior half	**Broad, triangular With transverse lines across entire width**
Dorsal flaps	Present	Absent	Present	Present	**Absent**
Posterior body region	Unknown	Tailfan, two pairs of caudal lobes	Tailfan, one pair of caudal lobes	No tailfan Trapezoidal termination	**Unknown**
References	Van Roy et al. 2015	Moysiuk & Caron, 2019	Daley et al. 2009, 2013; Van Roy et al. 2015	Whittington & Briggs 1985; Van Roy et al. 2015	**This study**

2   [1] does not include reduced anterior segments bearing lamellar bands known in *Cambroraster* and *Hurdia*.

Table 2. Taxonomic diversity and fossil richness of the radiodont faunas from the Cambrian Konservat-Lagerstätten of western Utah, USA.

Fossil richness is based on published data. Abbreviations used: AB, articulated body (+/-complete), CE, central carapace element, FA, frontal appendage, LE, lateral carapace element, OC, oral cone.

1 Table 2. Taxonomic diversity and fossil richness of the radiodont faunas from the Cambrian
2 Konservat-Lagerstätten of western Utah, USA. Fossil richness is based on published data.
3 Abbreviations used: AB, articulated body (+/- complete), CE, central carapace element, FA,
4 frontal appendage, LE, lateral carapace element, OC, oral cone.

Genus	Wheeler-HR	Wheeler-DM	Marjum	Weeks
Amplectobelua	*Amplectobelua* cf. *A. stephenensis* – 1 FA (*Lerosey-Aubril et al. 2020*)	Absent	Absent	Absent
Anomalocaris	Absent [1]	Absent [2]	Absent	*Anomalocaris* aff. *A. canadensis* – 5 FA *Anomalocaris* sp. – 1 FA (*Lerosey-Aubril et al. 2014*)
Buccaspinea	*B. cooperi*? – 1 FA (*Lerosey-Aubril et al. 2020a*, their '*Hurdia* sp. nov. A'; this study)	Absent	*B. cooperi* – 1 AB (This study)	Absent
Caryosyntrips	*C. serratus* – 2 FA (*Pates & Daley, 2017; Lerosey-Aubril et al. 2020a*)	*C. durus* – 2 FA (*Pates & Daley, 2017*)	*Caryosyntrips camurus* – 2 FA (This study)	Absent
Pahvantia	*Pa. hastata* – 1 FA, 14 CE, 9 LE (*Robison & Richards, 1981; Lerosey-Aubril & Pates, 2018; Lerosey-Aubril et al. 2020a*)	*Pa. hastata* – 1 CE (*Lerosey-Aubril & Pates, 2018*)	*Pa. hastata* – 3 CE (This study)	Absent
Peytoia	*Pe. nathorsti* – 1 FA, 3 OC (*Conway Morris & Robison 1982; Pates et al. 2018a*)	Absent	*Pe. nathorsti* – 1 AB, 1 OC (*Briggs & Robison, 1984; Pates et al. 2018a*)	Absent
Stanleycaris	*Stanleycaris* sp. – 1 FA (*Pates et al. 2017*)	Absent	Absent	Absent
New genus	Absent	Anomalocarididae gen. et sp. nov. – 1 FA (*Halgedahl et al. 2009*)	Absent	Absent

6 [1] *Briggs et al. (2008)* described an articulated body assigned to *Anomalocaris* from the Wheeler-HR. This specimen is currently under study and
7 is not thought to belong to the genus *Anomalocaris*.

8 [2] *Robison et al. 2015* listed the genus as present in the Wheeler-DM, referring to *Briggs et al. 2008*. In fact, the Wheeler specimens mentioned in
9 the latter publication were all from the Wheeler-HR.